Dalton Transactions

PAPER

View Article Online
View Journal | View Issue

Cite this: *Dalton Trans.*, 2014, **43**, 4653

Red emitting $[Ir(C^N)_2(N^N)]^+$ complexes employing bidentate 2,2′:6′,2″-terpyridine ligands for light-emitting electrochemical cells†

Edwin C. Constable,[a] Catherine E. Housecroft,*[a] Gabriel E. Schneider,[a] Jennifer A. Zampese,[a] Henk J. Bolink,*[b,c] Antonio Pertegás[b] and Cristina Roldan-Carmona[b]

Received 11th December 2013,
Accepted 19th January 2014

DOI: 10.1039/c3dt53477d

www.rsc.org/dalton

2,2′:6′,2″-Terpyridine (tpy), 4′-(4-HOC_6H_4)-2,2′:6′,2″-terpyridine (**1**), 4′-(4-$MeOC_6H_4$)-2,2′:6′,2″-terpyridine (**2**), 4′-(4-$MeSC_6H_4$)-2,2′:6′,2″-terpyridine (**3**), 4′-(4-$H_2NC_6H_4$)-2,2′:6′,2″-terpyridine (**4**) and 4′-(4-pyridyl)-2,2′:6′,2″-terpyridine (**4**) act as N^N chelates in complexes of the type $[Ir(C^N)_2(N^N)][PF_6]$ in which the cyclometallating ligand, C^N, is derived from 2-phenylpyridine (Hppy) or 3,5-dimethyl-1-phenyl-1*H*-pyrazole (Hdmppz). The single crystal structures of eight complexes have been determined, and in each iridium(III) complex cation, the non-coordinated pyridine ring of the tpy unit is involved in a face-to-face π-stacking interaction with the cyclometallated ring of an adjacent ligand. Solution NMR spectra of the $[Ir(ppy)_2(N^N)]^+$ complexes are consistent with the presence of a non-classical hydrogen bond between the non-coordinated N-donor of the tpy domain and a CH unit of one pyridine ring of an adjacent ppy^- ligand; the presence of the N···HC interaction was confirmed in one of the solid-state structures. The pendant pyridine ring of the coordinated tpy undergoes hindered rotation on the NMR timescale at 295 K. In CH_2Cl_2, the complexes are orange or red emitters, with λ_{max}^{em} in the range 580 to 642 nm; photoluminescence quantum yields (PLQY) are <10%, and lifetimes range from 54 to 136 ns. N-Methylation of the pendant 4′-(4-pyridyl) group in $[Ir(dmppz)_2(pytpy)][PF_6]$ essentially quenches the emission. Light-emitting electrochemical cells (LECs) have been fabricated in a thin film configuration; the emission spectra of the LECs are red-shifted with respect to the PL spectra of the corresponding complex in thin film configuration. For the device incorporating $[Ir(ppy)_2(pytpy)][PF_6]$, the PL to EL red-shift is extremely large and this is indicative of a different emitting state being involved. The most efficient devices used $[Ir(ppy)_2(\mathbf{1})][PF_6]$, $[Ir(ppy)_2(\mathbf{2})][PF_6]$ or $[Ir(ppy)_2(\mathbf{3})][PF_6]$ in the emissive layer; the devices exhibited rapid turn-on times, but showed relatively low efficiencies in accordance with the solid state photoluminescence quantum yields.

Introduction

The luminescent properties of cationic iridium(III) complexes of the type $[Ir(C^N)_2(N^N)]^+$ in which C^N is a cyclometallating ligand (*e.g.* the conjugate base of 2-phenylpyridine, Hppy) and N^N is 2,2′-bipyridine (bpy) or a derivative thereof have inspired their use as the ionic-transition metal complex (iTMC) component in light-emitting electrochemical cells (LECs).[1,2] In $[Ir(C^N)_2(N^N)]^+$ cations, the character of the highest occupied molecular orbital (HOMO) is a combination of iridium dπ and C^N ligand orbitals, while the lowest unoccupied molecular orbital (LUMO) is localized on the N^N ligand. This localization of orbital character allows the energies of the HOMO and LUMO (and hence the HOMO–LUMO gap), and thus the emission colour, to be tuned by judicious choice of substituents on the C^N and/or N^N ligands.[2] While an ability to colour-tune the emission of the iTMC is essential to its application in a LEC, achieving a long-lived device is also crucial. We have approached the latter by designing $[Ir(C^N)_2(N^N)]^+$ complexes in which there are inter-ligand π-stacking interactions.[3–6] The introduction of an aryl substituent into the 6-position of the bpy ligand results in the evolution of an intramolecular face-to-face π-interaction between

[a]*Department of Chemistry, University of Basel, Spitalstrasse 51, CH-4056 Basel, Switzerland. E-mail: catherine.housecroft@unibas.ch*
[b]*Instituto de Ciencia Molecular, Universidad de Valencia, C/Catedrático J. Beltrán 2, ES-46980 Paterna, Valencia, Spain*
[c]*Fundacion General de la Universidad de Valencia (FGUV), Spain*

†Electronic supplementary information (ESI) available: Fig. S1–S7, Fig. S9: ORTEP representations of complexes; Fig. S8. ^{1}H NMR spectrum of $[Ir(ppy)_2(Me\text{-}pytpy)][PF_6]_2$; Fig. S10. Representative cyclic voltammograms; Fig. S11. Device performance of $[Ir(ppy)_2(6\text{-}Phbpy)][PF_6]$ for comparison; Fig. S12. Thin film PL spectra. CCDC 974016–974023. For ESI and crystallographic data in CIF or other electronic format see DOI: 10.1039/c3dt53477d

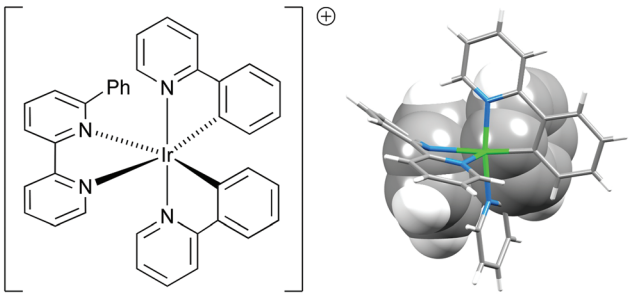

Fig. 1 Schematic representation of $[Ir(ppy)_2(6\text{-Phbpy})]^+$ and structural figure showing the face-to-face stacking of the phenyl substitution and phenyl ring of one $[ppy]^-$ ligand.

the aryl ring and the phenyl ring of one of the C^N ligands.[3,7–10] A LEC incorporating the iTMC $[Ir(ppy)_2(6\text{-Phbpy})]^+$ (Fig. 1, 6-Phbp = 6-phenyl-2,2′-bipyridine) exhibits a device lifetime of more than 3000 hours at an average luminance of 200 cd m^{-2} (driving voltage of 3 V),[3] and this is attributed to the formation of a cage-like arrangement of ligands that prevents expansion of the coordination sphere in the excited state, thereby inhibiting attack at the iridium centre by water with subsequent quenching. Since our initial report of this effect,[3] N^N ligands with pendant 6-substituted aryl groups have become a standard design feature of our iTMCs.[11–15] Interestingly, modifying the substitution pattern of the bpy ligand to permit two π-stacking interactions within the coordination sphere does not further enhance the device lifetime.[16]

In contrast to the wide range of bpy- or substituted bpy-containing $[Ir(C^N)_2(N^N)]^+$ complexes reported,[2] only two well-characterized examples of $[Ir(C^N)_2(N^N)]^+$ cations in which N^N is a derivative of 2,2′:6′,2″-terpyridine (tpy) have been described.[7,17] Room temperature, degassed MeCN solutions of $[Ir(ppy)_2(4'\text{-tolyltpy})][PF_6]$ (4′-tolyltpy = 4′-(4-tolyl)-2,2′:6′,2″-terpyridine) show an emission maximum in the red-orange region (λ_{max}^{em} = 625 nm) which shifts to 560 nm at 77 K in MeOH–EtOH. The related complex $[Ir(ppy)_2(4'\text{-}HO_2CC_6H_4tpy)][PF_6]$ emits at 632 nm in MeCN at room temperature, and at 615 nm in a solid film.[17] No structural data are available for these compounds, and a search of the Cambridge Structural Database[18] (v. 5.34 with November 2012 updates, using Conquest v. 1.15[19]) reveals no structures of complexes containing an $\{Ir(ppy)_2(tpy)\}$-unit. The preferred octahedral geometry of iridium(III) should dictate a bidentate mode for the tpy ligand in $[Ir(C^N)_2(tpy)]^+$ cations, leaving a pendant pyridine ring that can engage in a face-to-face π-interaction analogous to that shown for the phenyl rings in Fig. 1.

In this paper, we describe a series of $[Ir(ppy)_2(N^N)]^+$ complexes in which N^N is a tpy ligand. With the known orange-red emission[7] of $[Ir(ppy)_2(4'\text{-tolyltpy})]^+$ as a starting point, this family of complexes appeared suited for achieving deep red emitters. To date, red-emitting $[Ir(C^N)_2(N^N)]^+$ complexes which have been reported include those with photoluminescence emission maxima (in solution) of ≈650,[20] 656[21] and 687 nm,[22] and more recently, two red-emitting $[Ir(C^N)_2(N^N)]^+$ complexes containing 1,3,4-oxadiazole ligands and giving high efficiency LECs.[23] To achieve a smaller HOMO–LUMO gap and a longer wavelength emission, the HOMO should be destabilized and/or the LUMO stabilized.[2] In the first series of complexes discussed here, the C^N ligand is maintained as $[ppy]^-$, leading to an effectively constant HOMO level. The energy of the LUMO may be lowered by introducing electron-withdrawing substituents into the N^N ligand or extending the π-conjugation in the latter. The N^N ligands (Scheme 1) selected for this study were the parent tpy, ligands **1–4** which contain an extended π-system and a remote electron-withdrawing group, and 4′-pyridyl-2,2′:6′,2″-terpyridine (pytpy) in which the π-system extends to the additional pyridine ring. For $[Ir(C^N)_2(tpy)]^+$ and $[Ir(C^N)_2(pytpy)]^+$, we also investigate the effects of changing the C^N ligand from $[ppy]^-$ to $[dmppz]^-$ (Hdmppz = 3,5-dimethyl-1-phenyl-1*H*-pyrazole).

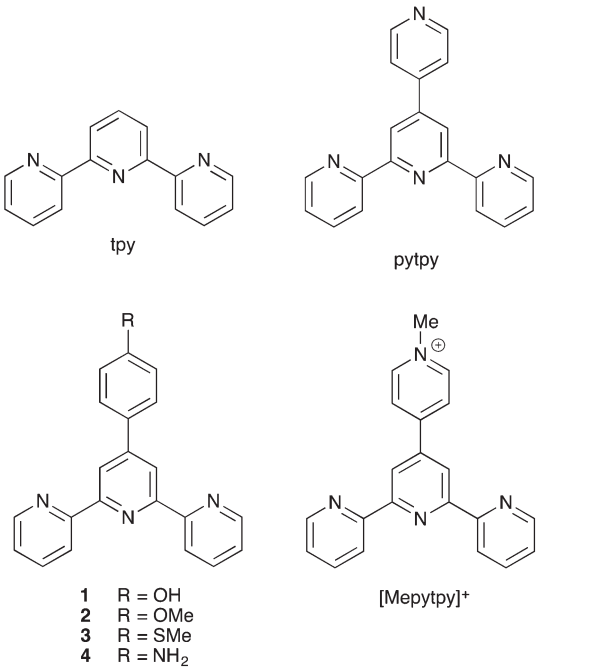

Scheme 1 Structures of the N^N ligands.

Experimental

General

^1H and ^{13}C NMR spectra were recorded using a Bruker Avance III-500 NMR spectrometer at 295 K unless otherwise stated; chemical shifts were referenced to residual solvent peaks with respect to δ(TMS) = 0 ppm. Electrospray ionization (ESI) mass spectra were recorded on a Bruker esquire 3000^{plus} instrument. Solution absorption and emission spectra were recorded on an Agilent 8453 spectrophotometer and a Shimadzu RF-5301 PC spectrofluorometer, respectively. A Shimadzu 8400S instrument with Golden Gate accessory (solid samples) was used to record FT-IR spectra. Quantum yields were measured using a

Hamamatsu absolute PL quantum yield spectrometer C11347 Quantaurus-QY. Lifetimes were measured using a Hamamatsu Compact Fluorescence lifetime spectrometer C11367 Quantaurus-Tau; an LED light source with an excitation wavelength of 280 nm was used. Microwave reactions were carried out in a Biotage Initiator 8 reactor.

Electrochemical measurements were recorded using a CH Instruments 900B potentiostat with glassy carbon, a platinum wire and a silver wire as the working, counter, and reference electrodes, respectively. Samples were dissolved in HPLC grade MeCN ($\approx 10^{-4}$ mol dm^{-3}) containing 0.1 mol dm^{-3} [^{n}Bu$_4$N][PF$_6$] as the supporting electrolyte; all solutions were degassed with argon. Cp_2Fe was used as an internal reference.

Literature procedures were followed for the preparation of tpy,[24] pytpy,[25] [Mepytpy][PF$_6$],[26] **1**,[25] **2**,[25] **3**,[27] and **4**,[28] and the dimers [Ir$_2$(ppy)$_4$Cl$_2$] and [Ir$_2$(dmppz)$_4$Cl$_2$] were prepared by a standard method.[29]

[Ir(ppy)$_2$(tpy)][PF$_6$]. A yellow suspension of [Ir$_2$(ppy)$_4$Cl$_2$] (100.0 mg, 0.0933 mmol) and tpy (43.8 mg, 0.188 mmol) in MeOH (15 mL) was heated in a microwave reactor for 30 min at 120 °C (P = 13 bar). The orange solution was then cooled to room temperature, and an excess of solid NH_4PF_6 was added. The mixture was stirred for 30 min at room temperature and then evaporated to dryness. The product was purified using column chromatography (Merck alumina 90; CH_2Cl_2 changing to CH_2Cl_2–MeOH = 100 : 5), and was then redissolved in CH_2Cl_2–MeOH and over-layered with Et_2O. Pure product precipitated over a few days and [Ir(ppy)$_2$(tpy)][PF$_6$] was isolated as an orange solid (78.4 mg, 0.0892 mmol, 47.6%). ^{1}H NMR (500 MHz, CD_2Cl_2) δ/ppm 8.87 (br, 1H, H^{B6}), 8.54 (overlapping d, 2H, H^{F3+E3}), 8.21 (m, 2H, H$^{G6+E4/F4}$), 8.16 (td, J = 8.1, 1.6 Hz, 1H, H$^{F4/E4}$), 7.89 (m, 1H, H^{B3}), 7.84 (d, J = 7.9 Hz, 1H, H^{D3}), 7.81–7.77 (m, 3H, H$^{B4+D4+E6}$), 7.62 (dd, J = 7.8, 1.2 Hz, 1H, H^{A3}), 7.45 (dd, J = 7.7, 1.2 Hz, 1H, H^{F5}), 7.39 (m, 2H, H^{D6+E5}), 7.34 (dd, J = 7.8, 1.2 Hz, 1H, H^{C3}), 7.15 (m, 2H, H^{B5+G4}), 6.97 (m, 3H, H$^{A4+D5+G5}$), 6.76 (td, J = 7.5, 1.4 Hz, 1H, H^{A5}), 6.64 (m, 1H, H^{C4}), 6.53 (d, J = 7.7 Hz, 1H, H^{G3}), 6.33 (td, J = 7.5, 1.3 Hz, 1H, H^{C5}), 5.89 (dd, J = 7.7, 0.9 Hz, 1H, H^{A6}), 5.45 (m, 1H, H^{C6}). ^{13}C NMR (126 MHz, CD_2Cl_2) δ/ppm 168.7 (C^{D2}), 167.0 (C^{B2}), 163.4 (C^{F6}), 157.5 (C$^{E2/F2}$), 157.4 (C$^{E2/F2}$), 156.4 (C^{G2}), 152.9 (C^{B6}), 150.9 (C^{E6}), 150.4 (C^{C1}), 148.7 (C^{G6}), 148.4 (C^{D6}), 146.7 (C^{A1}), 143.6 (C^{A2}), 142.9 (C^{C2}), 140.4 (C^{F4}), 139.9 (C^{E4}), 138.7 (C$^{B4/D4}$), 138.6 (C$^{B4/D4}$), 136.9 (C^{G4}), 132.9 (C^{C6}), 131.1 (C^{A6}), 131.0 (C^{A5}), 130.5 (C^{C5}), 129.5 (C^{F5}), 128.2 (C^{E5}), 125.8 (C^{E3}), 125.2 (C^{A3}), 124.7 (C^{G5}), 124.6 (C^{F3}), 124.4 (C^{C3}), 123.3 (C^{B5}), 123.2 (2C, C^{A4+D5}), 123.1 (C^{G3}), 121.3 (C^{C4}), 119.9 (C$^{B3/D3}$), 119.8 (C$^{B3/D3}$). IR (ν/cm^{-1}) 3090 w, 2921 w, 2852 w, 2350 w, 1778 w, 1608 m, 1583 m, 1478 m, 1452 m, 1420 m, 1317 w, 1270 w, 1155 s, 1137 s, 1065 w, 1030 w, 991 w, 955 w, 886 w, 836 s, 825 s, 775 m, 757 s, 739 m, 729 m, 722 m, 697 m, 630 m, 602 s. ESI MS m/z 734.2 [M − PF$_6$]$^+$ (calc. 734.2). UV-Vis λ/nm (ε/dm^3 mol^{-1} cm^{-1}) (CH_2Cl_2, 2.50 × 10^{-5} mol dm^{-3}): 261 (48 700), 375 (6100). Emission (CH_2Cl_2, 2.50 × 10^{-5} mol dm^{-3}, λ_{exc} = 260 nm) λ_{max}^{em} = 590 nm. Found C 50.31, H 3.16, N 7.97; $C_{37}H_{27}F_6IrN_5P$ requires C 50.57, H 3.10, N, 7.97%.

[Ir(ppy)$_2$(1)][PF$_6$]. A yellow suspension of [Ir$_2$(ppy)$_4$Cl$_2$] (107.2 mg, 0.100 mmol) and **1** (64.7 mg, 0.199 mmol) in MeOH (15 mL) was heated in a microwave reactor for 2 h at 120 °C (P = 13 bar). The orange solution was cooled to room temperature, and excess solid NH_4PF_6 was added. The mixture was stirred for 30 minutes at room temperature, but no precipitate formed. An excess of $AgPF_6$ was added, the mixture was stirred for 1 h and then evaporated to dryness. The crude material was purified twice by column chromatography (Merck alumina 90, CH_2Cl_2 changing to CH_2Cl_2–MeOH–MeCN = 100 : 5 : 5, followed by Fluka silica 60; CH_2Cl_2 changing to CH_2Cl_2–MeOH = 100 : 3). [Ir(ppy)$_2$(**1**)][PF$_6$] was isolated as an orange solid (154.0 mg, 0.158 mmol, 79.5%). ^{1}H NMR (500 MHz, CD_2Cl_2) δ/ppm 8.98 (br, 1H, H^{B6}), 8.68 (d, J = 8.3 Hz, 1H, H^{E3}), 8.58 (d, J = 2.0 Hz, 1H, H^{F3}), 8.48 (br, 1H, H^{OH}), 8.21 (br, 1H, H^{G6}), 8.16 (ddd, J = 8.2, 7.7, 1.6 Hz, 1H, H^{E4}), 7.89 (m, 1H, H$^{B3/D3}$), 7.86 (m, 1H, H$^{B3/D3}$), 7.84–7.78 (m, 3H, H$^{B4+D4+E6}$), 7.59 (dd, J = 7.8, 1.2 Hz, 1H, H^{A3}), 7.56 (m, 2H, H^{H2}), 7.54 (d, J = 6.0 Hz, 1H, H^{D6}), 7.43 (d, J = 1.9 Hz, 1H, H^{F5}), 7.38 (m, 2H, H^{E5+C3}), 7.17 (m, 2H, H^{B5+G4}), 7.02–6.95 (m, 3H, H$^{D5+G5+A4}$), 6.80 (td, J = 7.5, 1.4 Hz, 1H, H^{A5}), 6.71 (d, J = 8.6 Hz, 2H, H^{H3}), 6.66 (ddd, J = 7.8, 7.3, 1.2 Hz, 1H, H^{C4}), 6.56 (br, 1H, H^{G3}), 6.38 (td, J = 7.5, 1.2 Hz, 1H, H^{C5}), 5.91 (m, 1H, H^{A6}), 5.53 (d, J = 7.5 Hz, 1H, H^{C6}). ^{13}C NMR (126 MHz, CD_2Cl_2) δ/ppm 168.7 (C^{D2}), 167.2 (C^{B2}), 160.4 (C^{F6}), 160.0 (C^{H4}), 157.5 (C^{F2}), 157.3 (C^{E2}), 155.5 (C^{G2}), 151.9 (C^{B6}), 151.1 (C^{F4}), 150.9 (C^{C1}), 150.8 (C^{E6}), 149.1 (C^{D6}), 148.2 (C^{G6}), 147.4 (C^{A1}), 143.7 (C^{A2}), 143.2 (C^{C2}), 139.8 (C^{E4}), 138.7 (C$^{B4/D4}$), 138.6 (C$^{B4/D4}$), 137.2 (C^{G4}), 132.5 (C^{C6}), 131.0 (C^{A5}), 130.9 (C^{A6}), 130.5 (C^{C5}), 129.4 (C^{H2}), 128.2 (C^{E5}), 126.0 (C^{H1}), 125.9 (C^{F5}), 125.8 (C^{E3}), 125.1 (2C, C^{A3+G5}), 124.6 (C^{C3}), 123.9 (C^{G3}), 123.8 (C^{B5}), 123.3 (C^{A4}), 123.2 (C^{D5}), 121.3 (C^{C4}), 120.9 (C^{F3}), 120.0 (2C, C^{B3+D3}), 117.5 (C^{H3}). IR (ν/cm^{-1}) 3043 (w, ν_{OH}), 2601 w, 2162 w, 1663 w, 1607 s, 1583 s, 1520 m, 1477 s, 1438 m, 1419 m, 1404 m, 1367 w, 1319 w, 1285 m, 1270 m, 1233 m, 1163 m, 1042 m, 1031 m, 1025 m, 1009 m, 830 s, 828 s, 805 s, 790 s, 755 s, 739 s, 730 s, 627 s, 618 s. ESI MS m/z 826.3 [M − PF$_6$]$^+$ (calc. 826.2). UV-Vis (CH_2Cl_2, 1.00 × 10^{-5} mol dm^{-3}): λ/nm (ε/dm^3 mol^{-1} cm^{-1}) 256 (52 700), 364 (26 600). Emission (CH_2Cl_2, 1.00 × 10^{-5} mol dm^{-3}, λ_{exc} = 360 nm): λ_{max}^{em} = 590 nm. Found C 48.92, H 3.37, N 6.61; $C_{43}H_{31}F_6IrN_5OP{\cdot}4H_2O$ requires C 49.52, H 3.77, N 6.71%.

[Ir(ppy)$_2$(2)][PF$_6$]. The method was the same as that for [Ir(ppy)$_2$(**1**)][PF$_6$] starting with [Ir$_2$(ppy)$_4$Cl$_2$] (107.2 mg, 0.100 mmol) and **2** (67.5 mg, 0.199 mmol). The product was purified twice by column chromatography (Merck alumina 90 and then Fluka silica 60; CH_2Cl_2 changing to CH_2Cl_2–MeOH = 100 : 2 for both columns). [Ir(ppy)$_2$(**2**)][PF$_6$] was isolated as an orange solid (159 mg, 0.162 mmol, 81.2%). ^{1}H NMR (500 MHz, CD_2Cl_2) δ/ppm 8.89 (br, 1H, H^{B6}), 8.67 (d, J = 2.0 Hz, 1H, H^{F3}), 8.65 (d, J = 8.3 Hz, 1H, H^{E3}), 8.22 (broadened d, 1H, H^{G6}), 8.17 (ddd, J = 8.2, 7.7, 1.6 Hz, 1H, H^{E4}), 7.88–7.83 (overlapping m, 3H, H$^{B3+D3+H2}$), 7.78 (m, 3H, H$^{B4+D4+E6}$), 7.62 (m, 2H, H^{A3+F5}), 7.45 (d, J = 5.8 Hz, 1H, H^{D6}), 7.39 (ddd, J = 7.6, 5.5, 1.2 Hz, 1H, H^{E5}), 7.36 (dd, J = 7.8, 1.1 Hz, 1H, H^{C3}), 7.14 (m, 2H, H^{B5+G4}), 7.09 (m, 2H, H^{H3}), 6.97 (m, 2H, H^{A4+D5}), 6.93 (ddd, J = 7.6, 4.9, 0.9 Hz, 1H, H^{G5}), 6.77 (td, J = 7.5, 1.3 Hz, 1H, H^{A5}), 6.64

(m, 1H, H^{C4}), 6.55 (broadened d, 1H, H^{G3}), 6.34 (td, J = 7.4, 1.3 Hz, 1H, H^{C5}), 5.90 (dd, J = 7.8, 0.8 Hz, 1H, H^{A6}), 5.47 (dd, J = 7.6, 0.6 Hz, 1H, H^{C6}), 3.88 (s, 3H, H^{Me}). ^{13}C NMR (126 MHz, CD_2Cl_2) δ/ppm 168.8 (C^{D2}), 167.1 (C^{B2}), 163.6 (C^{F6}), 162.9 (C^{H4}), 157.8 (C^{F2}), 157.5 (C^{E2}), 156.6 (C^{G2}), 152.8 (C^{B6}), 151.5 (C^{F4}), 150.9 (C^{E6}), 150.6 (C^{C1}), 148.5 (C^{D6}), 148.3 (C^{G6}), 147.3 (C^{A1}), 143.7 (C^{A2}), 142.8 (C^{C2}), 139.8 (C^{E4}), 138.6 ($C^{B4/D4}$), 138.5 ($C^{B4/D4}$), 137.1 (C^{G4}), 132.8 (C^{C6}), 131.1 (C^{A6}), 131.0 (C^{A5}), 130.5 (C^{C5}), 129.4 (C^{H2}), 128.2 (C^{E5}), 127.5 (C^{H1}), 125.9 (C^{F5}), 125.7 (C^{E3}), 125.1 (C^{A3}), 124.6 (C^{G5}), 124.3 (C^{C3}), 123.3 (3C, $C^{A4+B5+G3}$), 123.2 (C^{D5}), 121.3 (C^{C4}), 121.1 (C^{F3}), 119.9 ($C^{B3/D3}$), 119.8 ($C^{B3/D3}$), 115.6 (C^{H3}), 56.2 (C^{Me}). IR (ν/cm^{-1}) 3042 w, 2344 w, 1700 m, 1603 s, 1583 s, 1517 m, 1476 s, 1459 m, 1437 m, 1424 m, 1420 m, 1410 m, 1399 m, 1366 w, 1303 m, 1268 m, 1247 s, 1231 m, 1181 m, 1164 m, 1122 w, 1095 w, 1065 w, 1030 m, 1003 m, 994 w, 879 w, 828 s, 828 s, 804 s, 788 s, 753 s, 727 s. ESI MS m/z 840.3 $[M - PF_6]^+$ (calc. 840.2). UV-Vis λ/nm (ε/dm^3 mol^{-1} cm^{-1}) (CH_2Cl_2, 1.00 × 10^{-5} mol dm^{-3}) 258 (42 200), 274 (42 700), 365 (15 300), 386 (10 500). Emission (CH_2Cl_2, 1.00 × 10^{-5} mol dm^{-3}, λ_{exc} = 320 nm) λ_{max}^{em} = 589 nm. Found C 52.55, H 3.40, N 6.92; $C_{44}H_{33}F_6IrN_5OP{\cdot}H_2O$ requires C 52.69, H 3.52, N, 6.98%.

[Ir(ppy)$_2$(3)][PF$_6$]. The method was the same as that for [Ir(ppy)$_2$(**1**)][PF$_6$] starting with [Ir$_2$(ppy)$_4$Cl$_2$] (107.2 mg, 0.100 mmol) and **3** (70.7 mg, 0.199 mmol). Chromatographic purification was the same as that for [Ir(ppy)$_2$(**2**)][PF$_6$]. [Ir(ppy)$_2$(**3**)][PF$_6$] was isolated as a pale orange solid (180.0 mg, 0.179 mmol, 90.2%). ^{1}H NMR (500 MHz, CD_2Cl_2) δ/ppm 8.86 (br, 1H, H^{B6}), 8.70 (d, J = 1.9 Hz, 1H, H^{F3}), 8.66 (d, J = 8.2 Hz, 1H, H^{E3}), 8.23 (d, J = 4.7 Hz, 1H, H^{G6}), 8.17 (td, J = 8.0, 1.6 Hz, 1H, H^{E4}), 7.88 (m, 2H, H^{B3+D3}), 7.80 (m, 5H, $H^{B4+D4+E6+H2}$), 7.65 (s, 1H, H^{F5}), 7.62 (dd, J = 7.9, 1.1 Hz, 1H, H^{A3}), 7.46 (d, J = 5.5 Hz, 1H, H^{D6}), 7.41 (m, 3H, H^{C3+H3}), 7.37 (dd, J = 7.8, 1.0 Hz, 1H, H^{E5}), 7.16 (m, 2H, H^{B5+G4}), 6.98 (m, 3H, $H^{A4+D5+G5}$), 6.78 (td, J = 7.5, 1.3 Hz, 1H, H^{A5}), 6.65 (td, J = 7.8, 1.2 Hz, 1H, H^{C4}), 6.57 (broadened d, 1H, H^{G3}), 6.35 (td, J = 7.5, 1.2 Hz, 1H, H^{C5}), 5.90 (dd, J = 7.7, 0.9 Hz, 1H, H^{A6}), 5.49 (d, J = 7.8 Hz, 1H, H^{C6}), 2.55 (s, 3H, H^{Me}). ^{13}C NMR (126 MHz, CD_2Cl_2, 298 K) δ/ppm 168.7 (C^{D2}), 167.1 (C^{B2}), 157.9 (C^{F2}), 157.4 (C^{E2}), 152.8 (C^{G2}), 152.6 (C^{B6}), 151.3 (C^{F4}), 150.9 (C^{E6}), 150.5 (C^{C1}), 148.6 (C^{D6}), 148.1 (C^{G6}), 147.2 (C^{A1}), 144.3 (C^{H4}), 143.7 (C^{A2}), 142.9 (C^{C2}), 139.8 (C^{E4}), 138.7 ($C^{B4/D4}$), 138.6 ($C^{B4/D4}$), 136.9 (C^{G4}), 132.9 (C^{C6}), 131.3 (C^{H1}), 131.1 (C^{A6}), 131.0 (C^{A5}), 130.5 (C^{C5}), 128.4 (C^{E5}), 128.1 (C^{H2}), 126.8 (C^{H3}), 126.3 (C^{F5}), 125.8 (C^{E3}), 125.1 (C^{A3}), 124.8 (C^{G5}), 124.4 (C^{C3}), 123.4 (2C, C^{B5+G3}), 123.3 (C^{A4}), 123.2 (C^{D5}), 121.3 (2C, C^{C4+F3}), 119.9 ($C^{B3/D3}$), 119.8 ($C^{B3/D3}$), 15.3 (C^{Me}); signal for C^{F6} not resolved. IR (ν/cm^{-1}) 3038 w, 1700 w, 1607 s, 1583 s, 1565 m, 1476 s, 1420 m, 1393 m, 1364 w, 1317 w, 1307 w, 1269 w, 1255 w, 1228 w, 1164 m, 1099 m, 1064 w, 1030 m, 993 w, 960 w, 879 w, 831 s, 831 s, 785 m, 753 s, 727 s, 710 m, 666 w, 627 s, 610 s, 603 m. ESI MS m/z 856.3 $[M - PF_6]^+$ (calc. 856.2). UV-Vis λ/nm (ε/dm^3 mol^{-1} cm^{-1}) (CH_2Cl_2, 1.00 × 10^{-5} mol dm^{-3}) 256 (52 700), 288 (41 200), 343 (26 100), 364 (26 600), 372 (25 700), 394 (18 000). Emission (CH_2Cl_2, 1.00 × 10^{-5} mol dm^{-3}, λ_{exc} = 325 nm) λ_{max}^{em} = 595 nm. Found C 51.41, H 3.27, N 6.81; $C_{44}H_{33}F_6IrN_5PS{\cdot}H_2O$ requires C 51.86, H 3.46, N, 6.87%.

[Ir(ppy)$_2$(4)][PF$_6$]. A yellow suspension of [Ir$_2$(ppy)$_4$Cl$_2$] (107.2 mg, 0.100 mmol) and **4** (65.7 mg, 0.201 mmol) in MeOH (15 mL) was heated in a microwave reactor for 2 h at 120 °C (P = 15 bar). The orange solution was then cooled to room temperature, and an excess of solid NH_4PF_6 was added. The mixture was stirred for 1 h at room temperature and then the solvent was evaporated to dryness. The crude orange product was dissolved in CH_2Cl_2 and the solution layered with Et_2O. After 2 days, the precipitate that had formed was separated by decanting the solvent, and [Ir(ppy)$_2$(**4**)][PF$_6$] was isolated as an orange-red solid (190 mg, 0.196 mmol, 97.2%). ^{1}H NMR (500 MHz, CD_2Cl_2) δ/ppm 8.90 (br, 1H, H^{B6}), 8.62 (m, 2H, H^{E3+F3}), 8.22 (broadened d, 1H, H^{G6}), 8.14 (m, 1H, H^{E4}), 7.87 (m, 2H, H^{B3+D3}), 7.79 (m, 3H, $H^{B4+D4+E6}$), 7.70 (m, 2H, H^{H2}), 7.62 (dd, J = 7.9, 1.2 Hz, 1H, H^{A3}), 7.56 (d, J = 2.0 Hz, 1H, H^{F5}), 7.45 (d, J = 5.7 Hz, 1H, H^{D6}), 7.36 (m, 2H, H^{E5+C3}), 7.14 (m, 1H, H^{B5}), 7.12 (td, J = 7.8, 1.8 Hz, 1H, H^{G4}), 6.96 (m, 2H, H^{A4+D5}), 6.92 (ddd, J = 7.6, 4.9, 1.1 Hz, 1H, H^{G5}), 6.80 (m, 2H, H^{H3}), 6.77 (m, 1H, H^{A5}), 6.64 (td, J = 7.7, 1.2 Hz, 1H, H^{C4}), 6.54 (broadened d, 1H, H^{G3}), 6.33 (m, 1H, H^{C5}), 5.91 (dd, J = 7.7, 0.9 Hz, 1H, H^{A6}), 5.47 (dd, J = 7.6, 0.7 Hz, 1H, H^{C6}), 3.65 (br, H^{NH_2}). ^{13}C NMR (126 MHz, CD_2Cl_2) δ/ppm 168.8 (C^{D2}), 167.1 (C^{B2}), 163.3 (C^{F6}), 157.7 (C^{E2}), 157.5 (C^{F2}), 156.7 (C^{G2}), 152.7 (C^{B6}), 151.6 (C^{F4}), 150.8 (2C, C^{E6+H4}), 150.7 (C^{C1}), 148.6 (C^{G6}), 148.4 (C^{D6}), 147.5 (C^{A1}), 143.7 (C^{A2}), 142.8 (C^{C2}), 139.7 (C^{E4}), 138.6 ($C^{B4/D4}$), 138.5 ($C^{B4/D4}$), 136.6 (C^{G4}), 132.8 (C^{C6}), 131.1 (C^{A6}), 130.9 (C^{A5}), 130.4 (C^{C5}), 129.2 (C^{H2}), 128.0 (C^{E5}), 125.5 (C^{E3}), 125.1 (C^{A3}), 124.9 (C^{F5}), 124.5 (C^{G5}), 124.3 (C^{C3}), 123.9 (C^{H1}), 123.3 (C^{B5}), 123.2 (C^{D5}), 123.1 (2C, C^{A4+G3}), 121.2 (C^{C4}), 120.1 (C^{F3}), 119.9 ($C^{B3/D3}$), 119.8 ($C^{B3/D3}$), 115.7 (C^{H3}). IR (ν/cm^{-1}) 3393 w, 3048 w, 2356 w, 1700 m, 1597 m, 1583 m, 1521 w, 1474 m, 1412 w, 1364 w, 1305 w, 1254 w, 1228 w, 1189 w, 1164 w, 1064 w, 1030 w, 1003 w, 942 w, 879 w, 828 s, 803 m, 788 m, 753 m, 728 m, 668 m, 602 s. ESI MS m/z 825.4 $[M - PF_6]^+$ (calc. 825.2). UV-Vis λ/nm (ε/dm^3 mol^{-1} cm^{-1}) (CH_2Cl_2, 1.00 × 10^{-5} mol dm^{-3}) 259 (52 100), 339 (24 800), 382 (25 500), 475 (2100). Emission (CH_2Cl_2, 1.00 × 10^{-5} mol dm^{-3}, λ_{exc} = 255 nm) λ_{max}^{em} = 580 nm. Found C 51.87, H 3.48, N 8.38; $C_{43}H_{32}F_6IrN_6P{\cdot}H_2O$ requires C 52.28, H 3.47, N, 8.51%.

[Ir(ppy)$_2$(pytpy)][PF$_6$]. A yellow suspension of [Ir$_2$(ppy)$_4$Cl$_2$] (107.6 mg, 0.100 mmol) and pytpy (62.4 mg, 0.201 mmol) in MeOH (15 mL) was heated in a microwave reactor for 30 min at 120 °C (P = 14 bar). The red solution was then cooled to room temperature, and an excess of solid NH_4PF_6 was added. The mixture was stirred for 1 h at room temperature, and the precipitate that formed was separated by filtration and washed with water (3 × 25 mL) and Et_2O (3 × 25 mL). The product was dissolved in CH_2Cl_2–MeOH and overlayered with n-hexane to give a red solid. This process was repeated, and the solid was then washed with Et_2O. [Ir(ppy)$_2$(pytpy)][PF$_6$] was isolated as a red solid (145 mg, 0.152 mmol, 76.1%). ^{1}H NMR (500 MHz, CD_2Cl_2) δ/ppm 8.94 (br, 1H, H^{B6}), 8.80 (d, J = 2.0 Hz, 1H, H^{F3}), 8.79 (m, 2H, H^{H2}), 8.75 (d, J = 8.3 Hz, 1H, H^{E3}), 8.25 (broadened d, 1H, H^{G6}), 8.19 (ddd, J = 8.1, 7.7, 1.6 Hz, 1H, H^{E4}), 7.91

(m, 1H, H^{B3}), 7.86 (m, 1H, H^{D3}), 7.84–7.76 (m, 5H, $H^{B4+D4+E6+H3}$), 7.67 (d, J = 1.9 Hz, 1H, H^{F5}), 7.64 (dd, J = 7.9, 1.2 Hz, 1H, H^{A3}), 7.44 (ddd, J = 5.9, 1.2, 0.5 Hz, 1H, H^{D6}), 7.42 (ddd, J = 7.6, 5.5, 1.2 Hz, 1H, H^{E5}), 7.37 (dd, J = 7.8, 1.1 Hz, 1H, H^{C3}), 7.15 (m, 2H, H^{B5+G4}), 6.97 (m, 3H, $H^{A4+D5+G5}$), 6.77 (m, 1H, H^{A5}), 6.65 (ddd, J = 7.8, 7.3, 1.2 Hz, 1H, H^{C4}), 6.60 (broadened d, 1H, H^{G3}), 6.34 (m, 1H, H^{C5}), 5.90 (dd, J = 7.7, 0.8 Hz, 1H, H^{A6}), 5.47 (dd, J = 7.6, 0.8 Hz, 1H, H^{C6}). ^{13}C NMR (126 MHz, CD_2Cl_2) δ/ppm 168.6 (C^{D2}), 167.0 (C^{B2}), 164.2 (C^{F6}), 158.6 (C^{F2}), 156.9 (C^{E2}), 156.2 (C^{G2}), 152.9 (C^{B6}), 151.1 (C^{H2}), 150.9 (C^{E6}), 150.3 (C^{C1}), 149.3 (C^{H4}), 148.9 (C^{G6}), 148.5 (C^{D6}), 146.9 (C^{A1}), 143.6 (2C, C^{A2+F4}), 142.9 (C^{C2}), 140.0 (C^{E4}), 138.7 ($C^{B4/D4}$), 138.6 ($C^{B4/D4}$), 136.7 (C^{G4}), 132.9 (C^{C6}), 131.1 (C^{A6}), 131.0 (C^{A5}), 130.5 (C^{C5}), 128.5 (C^{E5}), 126.9 (C^{F5}), 126.3 (C^{E3}), 125.2 (C^{A3}), 124.8 (C^{G5}), 124.3 (C^{C3}), 123.4 (2C, C^{A4+B5}), 123.3 (C^{D5}), 123.2 (C^{G3}), 122.2 (C^{H3}), 122.1 (C^{F3}), 121.4 (C^{C4}), 120.0 ($C^{B3/D3}$), 119.9 ($C^{B3/D3}$). IR (ν/cm^{-1}) 3043 w, 2344 w, 1607 m, 1583 m, 1535 w, 1477 m, 1439 w, 1419 m, 1398 m, 1316 w, 1270 w, 1228 w, 1164 w, 1065 w, 1031 w, 993 w, 879 w, 828 s, 788 m, 754 m, 728 m, 668 m, 624 m, 602 m. ESI MS m/z 811.3 $[M - PF_6]^+$ (calc. 810.9). UV-Vis λ/nm (ε/dm^3 mol^{-1} cm^{-1}) (CH_2Cl_2, 2.50 × 10^{-5} mol dm^{-3}): 258 (68 100), 350 (11 400). Emission (CH_2Cl_2, 2.50 × 10^{-5} mol dm^{-3}, λ_{exc} = 250 nm) λ_{max}^{em} = 640 nm. Found C 51.85, H 3.23, N 8.64; $C_{42}H_{32}F_6IrN_6P{\cdot}H_2O$ requires C 51.80, H 3.31, N, 8.63%.

[Ir(dmppz)$_2$(tpy)][PF$_6$]. The method and purification were the same as that for [Ir(ppy)$_2$(tpy)][PF$_6$], starting with [Ir$_2$(dmppz)$_4$Cl$_2$] (114.0 mg, 0.100 mmol) and tpy (46.9 mg, 0.201 mmol). [Ir(dmppz)$_2$(tpy)][PF$_6$] was isolated as an orange solid (179.2 mg, 196.2 mmol, 98.1%). ^{1}H NMR (500 MHz, CD_2Cl_2) δ/ppm 8.55 (dd, J = 8.2, 1.3 Hz, 1H, H^{F3}), 8.51 (d, J = 8.2 Hz, 1H, H^{E3}), 8.24 (t, J = 7.9 Hz, 1H, H^{F4}), 8.09 (m, 2H, H^{E4+G6}), 7.76 (ddd, J = 5.5, 1.6, 0.7 Hz, 1H, H^{E6}), 7.48 (dd, J = 7.7, 1.3 Hz, 1H, H^{F5}), 7.35 (ddd, J = 7.6, 5.5, 1.2 Hz, 1H, H^{E5}), 7.29 (dd, J = 8.2, 1.0 Hz, 1H, H^{A3}), 7.14 (td, J = 7.7, 1.7 Hz, 1H, H^{G4}), 6.97 (ddd, J = 8.1, 7.4, 1.4 Hz, 1H, H^{A4}), 6.92 (dd, J = 8.2, 0.8 Hz, 1H, H^{C3}), 6.85 (m, 2H, H^{G5}), 6.73 (m, 1H, H^{A5}), 6.57 (ddd, J = 8.2, 7.4, 1.4 Hz, 1H, H^{C4}), 6.42 (td, J = 7.4, 1.1 Hz overlapping br signal, 2H, H^{C5+G3}), 6.15 (s, 1H, H^{D4}), 6.05 (s, 1H, H^{B4}), 5.99 (dd, J = 7.6, 1.4 Hz, 1H, H^{A6}), 5.74 (dd, J = 7.5, 1.3 Hz, 1H, H^{C6}), 2.79 (s, 3H, $H^{Me\text{-}D3}$), 2.69 (s, 3H, $H^{Me\text{-}B3}$), 1.81 (s, 3H, $H^{Me\text{-}B5}$), 1.52 (s, 3H, $H^{Me\text{-}D5}$). ^{13}C NMR (126 MHz, CD_2Cl_2) δ/ppm 164.4 (C^{F6}), 157.8 ($C^{E2/F2}$), 157.6 ($C^{E2/F2}$), 154.9 (C^{G2}), 150.8 (C^{B5}), 150.5 (C^{D5}), 150.4 (C^{E6}), 148.9 (C^{G6}), 144.6 ($C^{A2/C2}$), 144.4 ($C^{A2/C2}$), 142.0 (C^{B3}), 141.5 (C^{D3}), 140.4 (C^{F4}), 139.7 (C^{E4}), 135.7 (C^{G4}), 134.4 (C^{C6}), 133.2 (C^{C1}), 133.0 (C^{A6}), 130.8 (C^{A1}), 130.3 (C^{F5}), 128.0 (C^{E5}), 126.2 (C^{A5}), 125.3 (C^{E3}), 124.9 (C^{C5}), 124.6 (C^{G5}), 123.9 (2C, C^{A4+F3}), 123.1 (C^{G3}), 121.9 (C^{C4}), 113.2 (C^{A3}), 112.6 (C^{C3}), 110.8 ($C^{B4/D4}$), 110.5 ($C^{B4/D4}$), 15.1 ($C^{Me\text{-}D3}$), 14.8 ($C^{Me\text{-}B3}$), 12.9 ($C^{Me\text{-}D5}$), 12.5 ($C^{Me\text{-}B5}$). IR (ν/cm^{-1}) 2920 w, 2366 w, 1988 w, 1696 w, 1604 w, 1568 w, 1553 m, 1471 m, 1445 w, 1428 w, 1397 w, 1372 w, 1312 w, 1296 w, 1274 w, 1234 w, 1192 w, 1167 w, 1150 w, 1122 w, 1075 w, 1036 w, 992 w, 925 w, 906 w, 884 w, 835 s, 823 m, 771 w, 744 m, 732 m, 717 m, 691 w, 636 m. ESI m/z 768.2 $[M - PF_6]^+$ (calc. 768.2). UV-Vis λ/nm (ε/dm^3 mol^{-1} cm^{-1}) (CH_2Cl_2, 2.50 × 10^{-5} mol dm^{-3}) 250 (53 000), 290 (33 300), 350 (7200). Emission (CH_2Cl_2, 2.50 × 10^{-5} mol dm^{-3}, λ_{exc} = 250 nm) λ_{max}^{em} = 599 nm. Found C 48.15, H 3.60, N 10.55; $C_{37}H_{33}F_6IrN_7P{\cdot}0.5H_2O$ requires C 48.21, H 3.72, N, 10.64%.

[Ir(dmppz)$_2$(pytpy)][PF$_6$]. The method was the same as that for [Ir(ppy)$_2$(**1**)][PF$_6$] starting with [Ir$_2$(dmppz)$_4$Cl$_2$] (114.0 mg, 0.100 mmol) and pytpy (62.4 mg, 0.201 mmol). The product was purified twice by column chromatography (Merck alumina 90 and then Fluka silica 60; CH_2Cl_2 changing to CH_2Cl_2–MeOH 100 : 5). [Ir(dmppz)$_2$(pytpy)][PF$_6$] was isolated as a red solid (135.0 mg, 0.136 mmol, 68.0%). ^{1}H NMR (500 MHz, CD_2Cl_2) δ/ppm 8.83 (m, 2H, H^{H2}), 8.79 (d, J = 2.0 Hz, 1H, H^{F3}), 8.72 (d, J = 8.2 Hz, 1H, H^{E3}), 8.13 (m, 2H, H^{E4+G6}), 7.82 (m, 2H, H^{H3}), 7.79 (ddd, J = 5.5, 1.6, 0.7 Hz, 1H, H^{E6}), 7.72 (d, J = 1.9 Hz, 1H, H^{F5}), 7.39 (m, 1H, H^{E5}), 7.31 (dd, J = 8.2, 1.0 Hz, 1H, H^{A3}), 7.16 (td, J = 7.7, 1.7 Hz, 1H, H^{G4}), 6.98 (ddd, J = 8.2, 7.4, 1.4 Hz, 1H, H^{A4}), 6.93 (dd, J = 8.2, 0.8 Hz, 1H, H^{C3}), 6.88 (m, 1H, H^{G5}), 6.74 (m, 1H, H^{A5}), 6.58 (ddd, J = 8.2, 7.4, 1.4 Hz, 1H, H^{C4}), 6.50 (br, 1H, H^{G3}), 6.44 (td, J = 7.4, 1.1 Hz, 1H, H^{C5}), 6.15 (s, 1H, H^{D4}), 6.06 (s, 1H, H^{B4}), 6.00 (dd, J = 7.6, 1.4 Hz, 1H, H^{A6}), 5.76 (dd, J = 7.5, 1.3 Hz, 1H, H^{C6}), 2.79 (s, 3H, $H^{Me\text{-}D3}$), 2.70 (s, 3H, $H^{Me\text{-}B3}$), 1.90 (s, 3H, $H^{Me\text{-}B5}$), 1.54 (s, 3H, $H^{Me\text{-}D5}$). ^{13}C NMR (126 MHz, CD_2Cl_2) δ/ppm 165.1 (C^{F6}), 159.0 (C^{F2}), 157.3 (C^{E2}), 154.7 (C^{G2}), 151.4 (C^{H2}), 150.8 (C^{B5}), 150.6 (C^{E6}), 150.5 (C^{D5}), 149.4 (C^{H4}), 149.1 (C^{G6}), 144.6 ($C^{A2/C2}$), 144.4 ($C^{A2/C2}$), 143.5 (C^{F4}), 142.1 (C^{B3}), 141.5 (C^{D3}), 139.9 (C^{E4}), 135.7 (C^{G4}), 134.5 (C^{C6}), 133.2 (C^{C1}), 133.0 (C^{A6}), 130.8 (C^{A1}), 128.3 (C^{E5}), 127.7 (C^{F5}), 126.3 (C^{A5}), 125.6 (C^{E3}), 125.0 (C^{C5}), 124.8 (C^{G5}), 124.0 (C^{A4}), 123.2 (C^{G3}), 122.1 (C^{H3}), 122.0 (C^{C4}), 121.4 (C^{F3}), 113.3 (C^{A3}), 112.6 (C^{C3}), 110.9 ($C^{B4/D4}$), 110.5 ($C^{B4/D4}$), 15.1 ($C^{Me\text{-}D3}$), 14.8 ($C^{Me\text{-}B3}$), 13.0 ($C^{Me\text{-}D5}$), 12.8 ($C^{Me\text{-}B5}$). IR (ν/cm^{-1}) 3131 w, 3054 w, 2162 w, 1700 m, 1585 m, 1549 m, 1541 m, 1471 s, 1442 m, 1420 m, 1398 s, 1373 m, 1276 m, 1263 m, 1239 m, 1168 w, 1143 m, 1068 w, 1037 m, 995 m, 903 m, 860 m, 830 s, 820 s, 792 s, 786 s, 753 s, 742 s, 730 s, 717 s, 703 s, 694 s, 659 m, 622 s, 612 s, 608 s. ESI MS m/z 845.3 $[M - PF_6]^+$ (calc. 845.3). UV-Vis λ/nm (ε/dm^3 mol^{-1} cm^{-1}) (CH_2Cl_2, 5.00 × 10^{-5} mol dm^{-3}) 253 (64 600), 320 (20 900), 350 (8400). Emission (CH_2Cl_2, 2.50 × 10^{-5} mol dm^{-3}, λ_{exc} = 256 nm) λ_{max}^{em} = 642 nm. Found C 48.64, H 3.53, N 10.53; $C_{42}H_{36}F_6IrN_8P{\cdot}2H_2O$ requires C 49.17, H 3.93, N, 10.92%.

[Ir(dmppz)$_2$(Mepytpy)][PF$_6$]$_2$. The method was the same as that for [Ir(ppy)$_2$(**1**)][PF$_6$] starting with [Ir$_2$(dmppz)$_4$Cl$_2$] (114.0 mg, 0.100 mmol) and [Mepytpy][PF$_6$] (98.8 mg, 0.21 mmol) with a reaction time of 90 min. The crude material was purified twice by column chromatography (Merck alumina 90 followed by Fluka silica 60; CH_2Cl_2 changing to CH_2Cl_2–MeOH = 100 : 4). [Ir(dmppz)$_2$(Mepytpy)][PF$_6$]$_2$ was isolated as a red solid (124.0 mg, 0.127 mmol, 63.6%). ^{1}H NMR (500 MHz, CD_2Cl_2) δ/ppm 9.03 (d, J = 2.0 Hz, 1H, H^{F3}), 8.88 (d, J = 8.3 Hz, 1H, H^{E3}), 8.80 (d, J = 6.9 Hz, 2H, H^{H2}), 8.60 (d, J = 7.0 Hz, 2H, H^{H3}), 8.14 (m, 2H, H^{E4+G6}), 7.85 (d, J = 1.9 Hz, 1H, H^{F5}), 7.79 (m, 1H, H^{E6}), 7.39 (ddd, J = 7.6, 5.5, 1.1 Hz, 1H, H^{E5}), 7.32 (dd, J = 8.2, 1.0 Hz, 1H, H^{A3}), 7.22 (m, 1H, H^{G4}), 6.98 (m, 1H, H^{A4}), 6.92 (m, 2H, H^{C3+G5}), 6.73 (m, 1H, H^{A5}), 6.63 (s, 1H, H^{G3}), 6.59 (m, 1H, H^{C4}), 6.45 (m, 1H, H^{C5}), 6.14 (s, 1H, H^{D4}), 6.07 (s, 1H,

H^{B4}), 5.99 (dd, J = 7.6, 1.3 Hz, 1H, H^{A6}), 5.76 (dd, J = 7.5, 1.3 Hz, 1H, H^{C6}), 4.47 (s, 3H, $H^{Me\text{-}H1}$), 2.78 (s, 3H, $H^{Me\text{-}D3}$), 2.71 (s, 3H, $H^{Me\text{-}B3}$), 1.93 (s, 3H, $H^{Me\text{-}B5}$), 1.53 (s, 3H, $H^{Me\text{-}D5}$). ^{13}C NMR (126 MHz, CD_2Cl_2, 298 K) δ/ppm 165.5 (C^{F6}), 160.0 (C^{F2}), 156.9 (C^{E2}), 154.0 (C^{G2}), 152.1 (C^{H4}), 151.1 (C^{B5}), 150.6 (C^{D5}), 150.4 (C^{E6}), 149.1 (C^{G6}), 146.3 (C^{H2}), 144.7 (C^{F4}), 144.5 ($C^{A2/C2}$), 144.3 ($C^{A2/C2}$), 142.1 (C^{B3}), 141.6 (C^{D3}), 140.1 (C^{E4}), 136.0 (C^{G4}), 134.6 (C^{C6}), 133.0 (2C, C^{A6+C1}), 130.4 (C^{A1}), 128.6 (C^{E5}), 128.1 (C^{F5}), 127.6 (C^{H3}), 126.5 (C^{E3}), 126.3 (C^{A5}), 125.1 (2C, C^{C5+G5}), 124.1 (C^{A4}), 123.4 (C^{G3}), 122.2 (C^{C4}), 122.1 (C^{F3}), 113.3 (C^{A3}), 112.6 (C^{C3}), 110.9 (C^{B4}), 110.6 (C^{D4}), 49.4 ($C^{Me\text{-}H1}$), 15.2 ($C^{Me\text{-}D3}$), 14.8 ($C^{Me\text{-}B3}$), 13.1 ($C^{Me\text{-}B5}$), 13.0 ($C^{Me\text{-}D5}$). IR (ν/cm^{-1}) 3657 w, 3131 w, 3054 w, 1646 w, 1617 w, 1570 w, 1553 w, 1528 w, 1471 s, 1444 w, 1414 w, 1398 w, 1375 w, 1337 w, 1276 w, 1270 w, 1225 w, 1195 w, 1146 w, 1122 w, 1093 w, 1059 w, 1035 w, 993 w, 822 s, 816 s, 789 s, 773 s, 743 s, 731 w, 719 w, 692 w, 657 w, 601 s. ESI MS m/z 1005.3 $[M - PF_6]^+$ (calc. 1005.3), 535.2 $[Ir(dmppz)_2]^+$ (calc. 535.2), 430.2 $[M - 2PF_6]^{2+}$ (calc. 430.2). UV-Vis λ/nm (ε/dm^3 mol^{-1} cm^{-1}) (CH_2Cl_2, 2.50 × 10^{-5} mol dm^{-3}) 256 (64 000), 315 (19 000), 400 (6000). Emission (CH_2Cl_2, 2.50 × 10^{-5} mol dm^{-3}, λ_{exc} = 245 nm) λ^{em}_{max} = 359 nm. Satisfactory elemental analysis was not obtained.

Crystallography

Data were collected on either a Bruker-Nonius KappaAPEX or a Stoe IPDS diffractometer with data reduction, solution and refinement using the program APEX2[30] or Stoe IPDS[31] software and SHELXL97.[32] Structures were analysed using Mercury v. 3.0.1[33,34] and the program was also used to draw the ORTEP-type figures. Crystallographic data are listed in Table 1.

Device preparation

The solvents were supplied by Aldrich. The thickness of films was determined using an Ambios XP-1 profilometer. ITO-coated glass plates (15 Ω □$^{-1}$) were patterned by conventional photolithography (http://www.naranjosubstrates.com) and substrates were cleaned by sonication in water-soap, water, and 2-propanol baths, in that order. After drying, the substrates were placed in a UV-ozone cleaner (Jelight 42-220) for 20 min.

To prepare the electroluminescence devices, an 80 nm layer of PEDOT : PSS (CLEVIOS™ P VP AI 4083, aqueous dispersion, 1.3–1.7% solid content, Heraeus) was first spin-coated onto the ITO glass substrate to improve device reproducibility and to prevent the formation of pinholes. Transparent films (90 nm thick) of the Ir complexes and the ionic liquid 1-butyl-3-methylimidazolium hexafluoridophosphate ([BMIM][PF_6], >98.5%, Sigma-Aldrich) in a 4 to 1 molar ratio were spin-coated from 20 mg cm^{-3} MeCN solution at 1000 rpm for 20 s. The devices were transferred in an inert atmosphere glovebox (<0.1 ppm O_2 and H_2O, MBraun) and were annealed at 100 °C for 1 h. The Al electrode (70 nm) was thermally evaporated using a shadow mask under a vacuum (<1 × 10^{-6} mbar) with an Edwards Auto500 evaporator integrated into the glovebox. The area of the device was 6.5 mm^2. The devices were not encapsulated and were characterized inside the glovebox at room temperature.

LEC characterization

Electroluminescence spectra were recorded using an Avantes fibre-optics photo-spectrometer Avaspec-2048. Device lifetimes were measured by applying pulsed currents and monitoring the voltage or current and luminance by a True Colour Sensor MAZeT (MTCSiCT Sensor) with a Botest OLT OLED Lifetime-Test System (for AC measurements) and a Keithley 2400 source meter and a photodiode coupled to a Keithley 6485 picometer using a Minolta LS100 to calibrate the photocurrent (for DC measurements).

Results and discussion

Syntheses of complexes and solution mass spectrometric and NMR spectroscopic characterizations

The complexes $[Ir(ppy)_2(N^N)][PF_6]$ (N^N = tpy, pytpy, **1–4**) and $[Ir(dmppz)_2(N^N)][PF_6]$ (N^N = tpy, pytpy) were prepared[35] by treating $[Ir_2(ppy)_4Cl_2]$ or $[Ir_2(dmppz)_4Cl_2]$ with two equivalents of the appropriate N^N ligand (Schemes 2 and 3). Yields were variable, ranging from 47.6% for $[Ir(ppy)_2(tpy)][PF_6]$ to 98.1% for $[Ir(dmppz)_2(tpy)][PF_6]$. In the ESI mass spectrum of each complex, the dominant peak envelope arose from the $[M - PF_6]^+$ ion and the observed isotope pattern matched that calculated.

The ^{1}H and ^{13}C NMR spectra of CD_2Cl_2 solutions of the complexes were recorded at room temperature, and were assigned using COSY, HMQC, HMBC and NOESY techniques. The aromatic regions of the ^{1}H NMR spectra of $[Ir(ppy)_2(N^N)][PF_6]$ with N^N = tpy, pytpy and ligands **1–4** appeared to be similar to one another and a representative example is shown in Fig. 2. An additional broad signal at δ 8.48 ppm in the aromatic region of the ^{1}H NMR spectrum of $[Ir(ppy)_2(\mathbf{1})][PF_6]$ was assigned to the OH proton of ligand **1**. The presence of the pendant pyridine ring (ring G) in each complex leads to non-equivalence of the two $[ppy]^-$ ligands. In Fig. 2, the two lowest frequency doublets arise from H^{A6} and H^{C6} of the cyclometallated rings, and the observed chemical shifts of these signals are typical of those observed in related complexes.[13] We have previously described the solution dynamic behaviour of complexes of type $[Ir(ppy)_2(PhN^N)]^+$,[13] $[Ir(dfppz)_2(PhN^N)]^+$ (Hdfppz = 1-(2,4-difluorophenyl)-1*H*-pyrazole),[14] and $[Ir(msppz)_2(PhN^N)]^+$ (Hmsppz = 1-(4-(methylsulfonyl)phenyl)-1*H*-pyrazole)[15] in which PhN^N is a 6-phenyl-2,2′-bipyridine ligand. In these complexes, the 6-phenyl substituent undergoes hindered rotation on the NMR timescale and the corresponding signals are typically broad or very broad at 298 K. In the solution ^{1}H NMR spectra of $[Ir(ppy)_2(tpy)][PF_6]$, $[Ir(ppy)_2(pytpy)][PF_6]$ and $[Ir(ppy)_2(\mathbf{4})][PF_6]$, the signals for H^{G3} and H^{G6} are slightly broadened; signals for H^{G4} and H^{G5} overlap with other resonances. More noticeable line broadening is observed in the spectra of $[Ir(ppy)_2(\mathbf{1})][PF_6]$, $[Ir(ppy)_2(\mathbf{2})][PF_6]$ and $[Ir(ppy)_2(\mathbf{3})][PF_6]$ (Fig. 2). The second significant difference

Table 1 Crystallographic data for the iridium(III) complexes

Compound	4{[Ir(ppy)$_2$(tpy)][PF$_6$]}·2.5Et$_2$O·1.5MeCN·3H$_2$O	4{[Ir(ppy)$_2$(**2**)][PF$_6$]}·Et$_2$O·2MeCN	2{[Ir(ppy)$_2$(**3**)][PF$_6$]}·MeCN·H$_2$O	[Ir(ppy)$_2$(**4**)][PF$_6$]·2CH$_2$Cl$_2$
Formula	$C_{161}H_{143.5}F_{24}Ir_4N_{21.5}O_{5.5}P_4$	$C_{184}H_{148}F_{24}Ir_4N_{22}O_5P_4$	$C_{90}H_{73}F_{12}Ir_2N_{11}O_2P_2S_2$	$C_{45}H_{36}Cl_4F_6IrN_6P$
Formula weight	3816.16	4096.00	2079.12	1139.79
Crystal colour and habit	Yellow block	Yellow block	Orange block	Orange plate
Crystal system	Triclinic	Monoclinic	Monoclinic	Monoclinic
Space group	$P\bar{1}$	$C2/c$	$P2_1/n$	$P2_1/n$
a, b, c/Å	13.770(2)	55.632(4)	14.5443(10)	10.2803(4)
	17.615(3)	10.5213(11)	14.7612(10)	12.4470(4)
	18.315(2)	34.013(2)	19.8943(14)	33.7717(12)
α, β, γ/°	85.763(12)	90	90	90
	85.821(11)	124.848(4)	104.707(4)	93.369(2)
	67.441(11)	90	90	90
U/Å^3	4086.4(10)	16 338(2)	4131.2(5)	4313.9(3)
Dc /Mg m^{-3}	1.548	1.665	1.668	1.755
Z	1	4	2	4
μ(Mo-Kα)/mm^{-1}	3.372	3.381	3.392	3.448
T/K	173	173	123	173
Refln. collected (R_{int})	93 421 (0.1519)	163 250 (0.0969)	134 040 (0.0425)	31 698 (0.0542)
Unique refln.	16 046	20 080	12 026	8021
Refln. for refinement	13 628	18 711	10 753	6667
Parameters	1048	1220	570	622
Threshold	$I > 2.0\sigma$	$I > 2.0\sigma$	$I > 2.0\sigma$	$I > 2.0\sigma$
R_1 (R_1 all data)	0.0523 (0.0605)	0.0286 (0.0320)	0.0194 (0.0247)	0.0476 (0.0637)
wR_2 (wR_2 all data)	0.1393 (0.1464)	0.0605 (0.0617)	0.0444 (0.0471)	0.0993 (0.1155)
Goodness of fit	1.080	1.195	1.047	1.151
CCDC deposition‡	974016	974020	974021	974019

Compound	2{[Ir(ppy)$_2$(pytpy)][PF$_6$]}·Et$_2$O·CH$_2$Cl$_2$	[Ir(dmppz)$_2$(tpy)][PF$_6$]	[Ir(dmppz)$_2$(pytpy)][PF$_6$]·CH$_2$Cl$_2$	[Ir(dmppz)$_2$(Mepytpy)][PF$_6$]$_2$·2CH$_2$Cl$_2$
Formula	$C_{89}H_{72}Cl_2F_{12}Ir_2N_{12}OP_2$	$C_{37}H_{33}F_6IrN_7P$	$C_{43}H_{38}Cl_2F_6IrN_8P$	$C_{45}H_{43}Cl_4F_{12}IrN_8P_2$
Formula weight	2070.87	912.89	1074.90	1319.83
Crystal colour and habit	Orange needle	Yellow block	Orange block	Red block
Crystal system	Triclinic	Monoclinic	Triclinic	Triclinic
Space group	$P\bar{1}$	$P2_1/n$	$P\bar{1}$	$P\bar{1}$
a, b, c/Å	10.641(2)	12.7713(7)	10.8170(7)	9.0099(16)
	18.025(4)	21.4055(16)	13.5418(8)	14.026(3)
	21.629(4)	12.8079(8)	14.6844(9)	20.222(5)
α, β, γ/°	88.86(3)	90	94.081(2)	101.420(16)
	82.15(3)	94.874(5)	100.297(2)	96.000(16)
	81.97(3)	90	103.316(2)	99.536(14)
U/Å^3	4069.3(14)	3488.7(4)	2045.2(2)	2445.4(8)
D_c/Mg m^{-3}	1.690	1.738	1.745	1.792
Z	2	4	2	2
μ(Mo-Kα)/mm^{-1}	3.457	3.944	8.510	3.104
T/K	173	173	123	173
Refln. collected (R_{int})	50 153 (0.2647)	93 669 (0.0726)	46 149 (0.0286)	26 234 (0.0704)
Unique refln.	14 413	10 141	7238	10 145
Refln. for refinement	9184	9710	7171	8551
Parameters	1084	473	554	682
Threshold	$I > 2.0\sigma$	$I > 2.0\sigma$	$I > 2.0\sigma$	$I > 2.0\sigma$
R_1 (R_1 all data)	0.0995 (0.1535)	0.0234 (0.0251)	0.0227 (0.0229)	0.0442 (0.0600)
wR_2 (wR_2 all data)	0.1963 (0.2328)	0.0575 (0.0582)	0.0596 (0.0598)	0.0879 (0.0926)
Goodness of fit	1.043	1.167	1.100	1.042
CCDC deposition‡	974018	974017	974022	974023

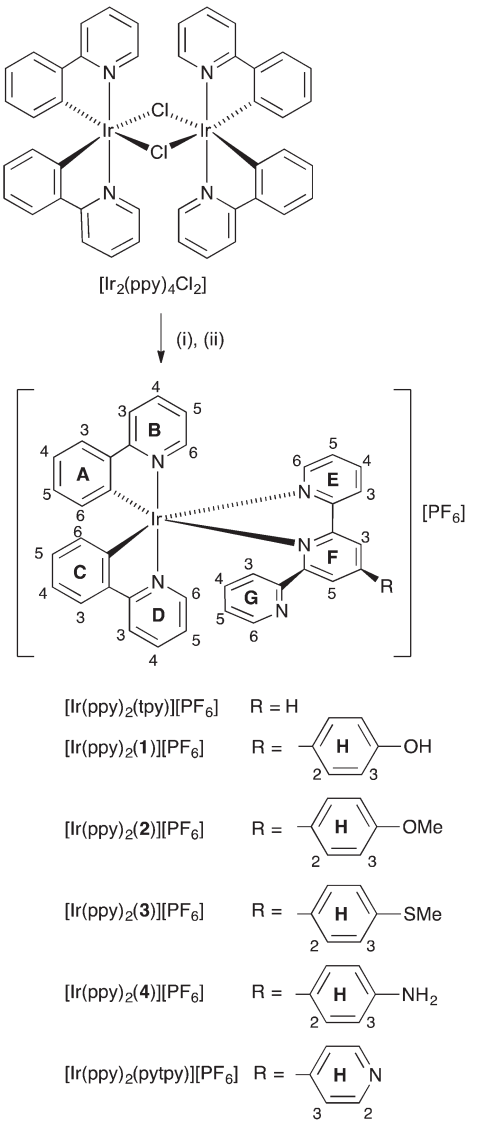

Scheme 2 Syntheses of $[Ir(ppy)_2(N\text{^}N)][PF_6]$ complexes. Conditions: (i) N^N ligand, MeOH, microwave reactor 120 °C, time (see the Experimental section); (ii) NH_4PF_6. Atom and ring labels used for NMR spectroscopic assignments are shown.

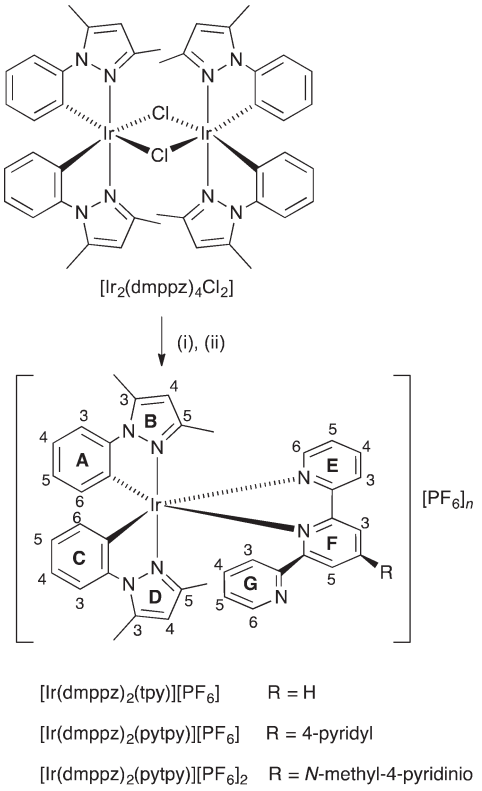

Scheme 3 Syntheses of $[Ir(dmppz)_2(N\text{^}N)][PF_6]_n$ complexes. Conditions: (i) N^N ligand, MeOH, microwave reactor 120 °C; (ii) NH_4PF_6. Atom and ring labels used for NMR spectroscopic assignments are shown.

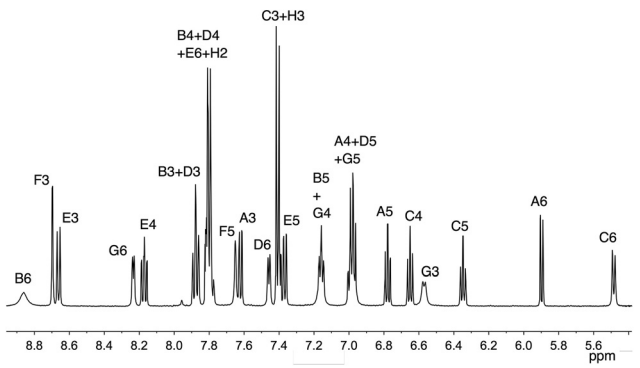

Fig. 2 500 MHz ^1H NMR spectrum of $[Ir(ppy)_2(\mathbf{3})][PF_6]$ in CD_2Cl_2 (295 K); the signal for the Me group is omitted. See Scheme 2 for atom labelling.

between the ^1H NMR spectra of the $[Ir(ppy)_2(PhN\text{^}N)]^+$ (ref. 13–15) and $[Ir(ppy)_2(tpy)]^+$ families is that the signal for H^{B6} is broad in the latter (Fig. 2) and is shifted to higher frequency with respect to the corresponding signal in $[Ir(ppy)_2(PhN\text{^}N)]^+$. This is rationalized by the formation of an N···HC hydrogen bond between the N atom of ring G and H^{B6}. Since ring G undergoes hindered rotation on the NMR timescale at room temperature, proton H^{B6} experiences more than one environment as the hydrogen bond is sequentially formed and broken. Note that no other signal for ring B protons is broadened. The presence of the N···HC interaction is confirmed in the solid-state structures of four of the complexes described below.

The essential differences between the aromatic regions of the ^1H NMR spectra of $[Ir(dmppz)_2(N\text{^}N)][PF_6]$ (N^N = tpy or pytpy) and $[Ir(ppy)_2(N\text{^}N)][PF_6]$ (N^N = tpy, pytpy, **1**–**4**) are in signals associated with rings B and D. Singlets at δ 6.15 and 6.05 ppm or at δ 6.15 and 6.06 ppm are assigned to H^{D4} and H^{B4} in $[Ir(dmppz)_2(tpy)][PF_6]$ and $[Ir(dmppz)_2(pytpy)][PF_6]$, respectively. No hydrogen-bonding interaction analogous to that seen in $[Ir(ppy)_2(N\text{^}N)]^+$ is possible in $[Ir(dmppz)_2(N\text{^}N)]^+$ because of the presence of the methyl substituents in ring B (but see the structural description below).

Crystal structure determinations

The single crystal structures of 4{[Ir(ppy)$_2$(tpy)][PF$_6$]}·2.5Et$_2$O·1.5MeCN·3H$_2$O, 4{[Ir(ppy)$_2$(**2**)][PF$_6$]}·Et$_2$O·2MeCN, 2{[Ir(ppy)$_2$(**3**)][PF$_6$]}·MeCN·H$_2$O, [Ir(ppy)$_2$(**4**)][PF$_6$]·2CH$_2$Cl$_2$ and 2{[Ir(ppy)$_2$(pytpy)][PF$_6$]}·Et$_2$O·CH$_2$Cl$_2$ were determined. Each complex crystallizes in a centrosymmetric space group with both enantiomers of the octahedral [Ir(ppy)$_2$(N^N)]$^+$ cation in the unit cell. Since the structures of the cations are similar, they are discussed together; ORTEP diagrams are shown in Fig. S1–S5.† In each [Ir(ppy)$_2$(N^N)]$^+$ cation, the N-donors of the cyclometallated ligands are mutually *trans*, and the bond distances within the iridium(III) coordination sphere (see captions to Fig. S1–S5†) are unexceptional. Each tpy ligand binds to the iridium(III) ion in a chelating manner and the third pyridine ring is involved in a face-to-face stacking interaction with the phenyl ring of one of the [ppy]$^-$ domains (Fig. 3). The parameters that define the π-interactions are given in Table 2 and confirm efficient contacts.[36] With the exception of [Ir(ppy)$_2$(**4**)]$^+$, the tpy domain in the cation adopts a *cis*,*cis*-conformation. The *cis*-arrangement of one pair of pyridine rings is necessitated by the chelating mode of the ligand. The *cis*-arrangement of the middle and pendant pyridine rings is a consequence of an intramolecular CH···N hydrogen bond. Fig. 4a shows the interaction in [Ir(ppy)$_2$(tpy)]$^+$, and hydrogen bond parameters for analogous contacts in the four complexes are listed in Table 3. Fig. 4b illustrates that in [Ir(ppy)$_2$(**4**)][PF$_6$]·2CH$_2$Cl$_2$, centrosymmetric pairs of cations associate through a combination of NH$_{amine}$···N$_{pyridine}$ hydrogen bonds (N···H = 2.68 Å) and face-to-face interactions between the aminophenylpyridine units of adjacent ligands **4** (interplane separation = 3.37 Å). Note that the NMR spectroscopic data discussed above are consistent with intramolecular hydrogen bonding in all five complexes.

Single crystals of [Ir(dmppz)$_2$(tpy)][PF$_6$] and [Ir(dmppz)$_2$(pytpy)][PF$_6$]·CH$_2$Cl$_2$ were grown from dichloromethane solutions of the compounds. The two complexes crystallize in the $P\bar{1}$ space group with both enantiomers of the octahedral cation in the unit cell. ORTEP representations of the [Ir(dmppz)$_2$(tpy)]$^+$ and [Ir(dmppz)$_2$(pytpy)]$^+$ cations are given in Fig. S6 and S7;† Ir–C and Ir–N bond distances are listed in the figure captions.† Consistent with expectations, the N-atoms of the cyclometallated [dmppz]$^-$ ligands are *trans* to one another, and the non-coordinated pyridine ring of the tpy domain is twisted with respect to the two coordinated rings to facilitate an intra-cation π-interaction (Fig. 5). The twist angles are 69.6° in [Ir(dmppz)$_2$(tpy)]$^+$ and 62.7° in [Ir(dmppz)$_2$(pytpy)]$^+$. For the face-to-face contacts between pyridine and cyclometallated rings, the angles between the ring planes and the distances between the ring centroids are 10.1° and 3.41 Å in [Ir(dmppz)$_2$(tpy)]$^+$, and 8.0° and 3.55 Å in [Ir(dmppz)$_2$(pytpy)]$^+$. These values compare favourably with those in Table 2. Fig. 5a also highlights a short CH$_{Me}$···N contact (2.70 Å) between the non-coordinated pyridine ring and a methyl substituent of one [dmppz]$^-$ ligand. The corresponding separation in [Ir(dmppz)$_2$(pytpy)]$^+$ is significantly longer (3.46 Å). The [Ir(dmppz)$_2$(pytpy)]$^+$ cations in [Ir(dmppz)$_2$(pytpy)][PF$_6$]·CH$_2$Cl$_2$ assemble into chains running along the *c*-axis supported by CH$_{dmppz}$···N$_{py}$ contacts (N$_{py}$ = 4′-pyridyl group) at a separation of 2.70 Å.

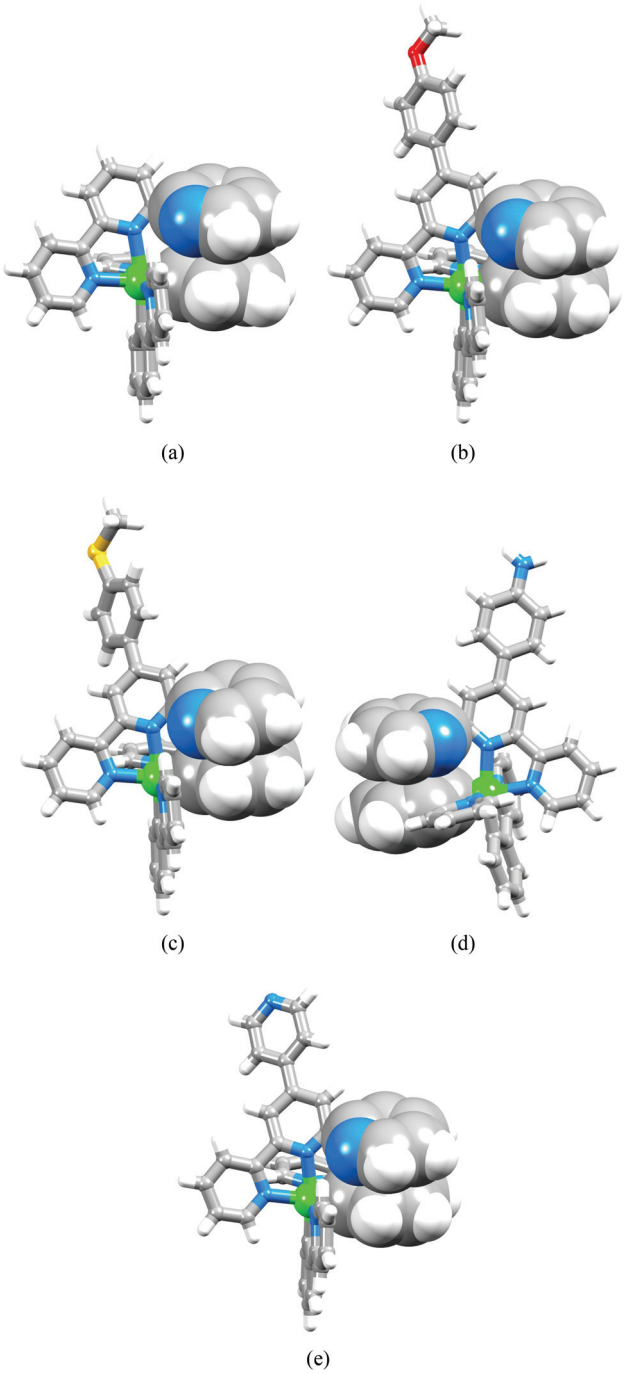

Fig. 3 Intra-cation π-interactions in (a) [Ir(ppy)$_2$(tpy)]$^+$ (one of two independent cations), (b) [Ir(ppy)$_2$(**2**)]$^+$ (one of two independent cations), (c) [Ir(ppy)$_2$(**3**)]$^+$, (d) [Ir(ppy)$_2$(**4**)]$^+$ and (e) [Ir(ppy)$_2$(pytpy)]$^+$ (one of two independent cations). Nitrogen atoms are shown in blue.

Synthesis and characterization of [Ir(dmppz)$_2$(Mepytpy)][PF$_6$]$_2$

The absorption and emission spectra of iron(II), ruthenium(II), osmium(II) and iridium(III) complexes containing pytpy ligands

Table 2 Comparison of the twist angle of the pendant pyridine ring and the structural parameters (in last two columns of the table) that define the face-to-face π-interactions in the $[Ir(ppy)_2(N\hat{}N)]^+$ cations (N^N = tpy, **2**, **3**, **4** and pytpy)

Cation	Twist angle between the middle and pendant py rings of the tpy unit/°	Angle between least squares planes of rings/°	Distance between ring centroids/Å
$[Ir(ppy)_2(tpy)]^+$	64.7	11.0	3.50
(2 independent cations)	62.0	7.2	3.45
$[Ir(ppy)_2(\mathbf{2})]^+$	64.4	3.4	3.49
(2 independent cations)	60.5	8.0	3.42
$[Ir(ppy)_2(\mathbf{3})]^+$	41.9	12.1	3.60
$[Ir(ppy)_2(\mathbf{4})]^+$	64.2	9.8	3.52
$[Ir(ppy)_2(pytpy)]^+$	50.7	8.3	3.54
(2 independent cations)	47.8	14.5	3.56

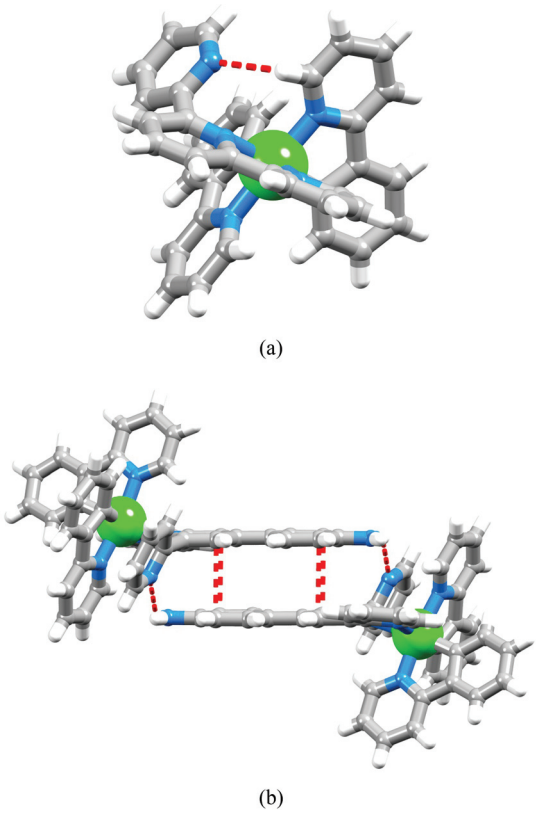

Fig. 4 (a) Intramolecular CH···N hydrogen bond in one of the independent $[Ir(ppy)_2(tpy)]^+$ cations in $4\{[Ir(ppy)_2(tpy)][PF_6]\}\cdot 2.5Et_2O\cdot 1.5MeCN\cdot 3H_2O$. (b) Association of centrosymmetric pairs of $[Ir(ppy)_2(\mathbf{4})]^+$ cations in $[Ir(ppy)_2(\mathbf{4})][PF_6]\cdot 2CH_2Cl_2$ through π-stacking and NH···N hydrogen bonds.

Table 3 Comparison of intramolecular hydrogen bond parameters (see Fig. 4) in the $[Ir(ppy)_2(N\hat{}N)]^+$ cations (N^N = tpy, **2**, **3**, **4** and pytpy)

Cation	CH···N/Å	C···N/Å	C–H···N/°
$[Ir(ppy)_2(tpy)]^+$	2.57	3.18(1)	122
(2 independent cations)	2.63	3.249(8)	123
$[Ir(ppy)_2(\mathbf{2})]^+$	2.55	3.116(5)	119
(2 independent cations)	2.55	3.185(4)	125
$[Ir(ppy)_2(\mathbf{3})]^+$	2.40	3.040(2)	124
$[Ir(ppy)_2(pytpy)]^+$	2.44	3.12(2)	128
(2 independent cations)	2.58	3.09(3)	114

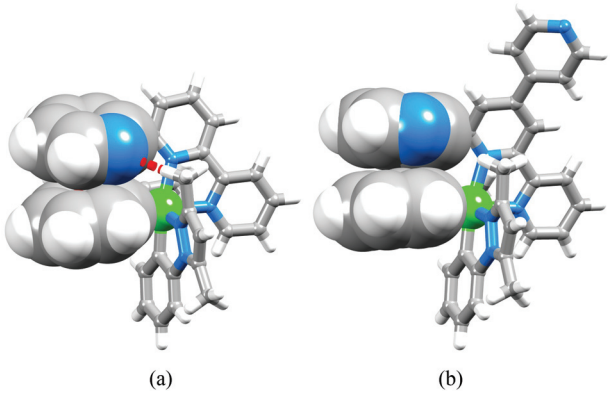

Fig. 5 Structures of (a) $[Ir(dmppz)_2(tpy)]^+$ showing π-stacking and $CH_{Me}\cdots N$ (in red) interactions, and (b) $[Ir(dmppz)_2(pytpy)]^+$ showing intramolecular π-stacking.

can be dramatically affected by protonation or methylation of the pendant pyridyl substituents.[37,38] We therefore prepared the *N*-methylated complex $[Ir(dmppz)_2(Mepytpy)]^{2+}$ for comparison with its non-methylated analogue. $[Ir(dmppz)_2(Mepytpy)][PF_6]_2$ was synthesized (Scheme 3) by a reaction of $[Ir_2(dmppz)_4Cl_2]$ with $[Mepytpy][PF_6]$.[26] After work-up, the product was isolated in 63.6% yield. The electrospray mass spectrum exhibited peak envelopes at *m*/*z* 1005.3 and 430.2 corresponding to $[M - PF_6]^+$ and $[M - 2PF_6]^{2+}$. Additionally, a peak at *m*/*z* 535.2 arising from $[Ir(dmppz)_2]^+$ was observed. The ^1H and ^{13}C NMR spectra (assigned by 2D methods) were in accord with the structure shown in Scheme 3. The solution ^1H NMR spectrum of $[Ir(dmppz)_2(Mepytpy)][PF_6]_2$ (Fig. S8†) exhibits a singlet at δ 4.47 ppm assigned to the *N*-Me group. Otherwise, the most significant changes on going from the spectrum of $[Ir(dmppz)_2(pytpy)][PF_6]$ to $[Ir(dmppz)_2(Mepytpy)][PF_6]_2$ are shifts to higher frequency for the signals arising from protons H^{H3} (δ 7.82 to 8.60 ppm), H^{F3} (δ 8.79 to 9.03 ppm), and H^{F5} (δ 7.72 to 7.85 ppm).

Single crystals of $[Ir(dmppz)_2(Mepytpy)][PF_6]_2\cdot 2CH_2Cl_2$ were grown from a dichloromethane solution of the complex. Crystallization in the $P\bar{1}$ space group leads to both enantiomers of the octahedral cation being present in the unit cell. Fig. S9† shows an ORTEP representation of the $[Ir(dmppz)_2(Mepytpy)]^{2+}$ cation, and gives Ir–C and Ir–N bond distances.† The structural determination confirms that the N-atoms of the cyclometallated ligands are mutually *trans*, and that the non-coordinated pyridine ring of the tpy unit twists through 78.2°, enabling it to engage in a π-stacking interaction with one of the cyclometallated phenyl rings (Fig. 6a); the angle between the ring planes is 8.4°, and the inter-centroid separation is 3.44 Å (both values are similar to those in $[Ir(dmppz)_2(pytpy)]^+$, see above). A short $CH_{Me}\cdots N$ contact (2.69 Å) mimics that in $[Ir(dmppz)_2(tpy)]^+$ (compare Fig. 5 and 6a). The *N*-methyl-

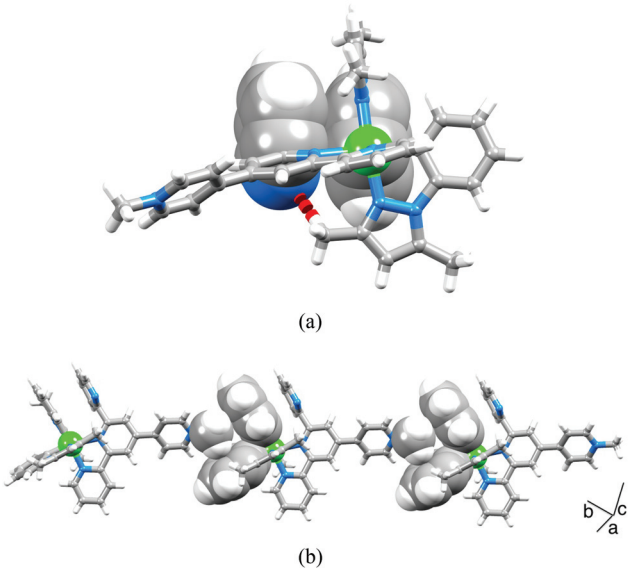

Fig. 6 (a) Structure of the $[Ir(dmppz)_2(Mepytpy)]^{2+}$ cation showing face-to-face π-stacking and $CH_{Me}\cdots N$ short contact (in red). (b) Cations assemble into chains through $\pi\cdots H_{Me}$ contacts.

pyridinio unit is directed into the V-shaped cavity formed by two of the cyclometallating ligands of an adjacent cation, and is involved in close $CH_{Me}\cdots\pi$ contacts (the shortest CH···centroid distances are 2.68 and 2.84 Å). This results in the assembly of chains (Fig. 6b) that run obliquely through the unit cell.

Electrochemistry

The iridium(III) complexes are all electrochemically active and Table 4 summarizes their redox behaviour. Each complex undergoes a quasi-reversible (Fig. S10†) or irreversible oxidation, assigned to an iridium-based process. The oxidation of $[Ir(ppy)_2(tpy)]^+$ occurs at slightly higher potential than that of $[Ir(ppy)_2(bpy)]^+$ (0.84 V).[39] Introduction of the 4′-aryl substituent on going from tpy to ligands **1–4** lowers the oxidation potential, consistent with the electron-releasing properties of the aromatic substituent. Oxidation of $[Ir(ppy)_2(pytpy)]^+$ occurs at a similar potential to that of $[Ir(ppy)_2(tpy)]^+$. Introduction of the electron-rich $[dmppz]^-$ ligands in place of $[ppy]^-$ lowers $E^{ox}_{1/2}$ by 0.08 V for $[Ir(C\text{^}N)_2(tpy)]^+$ and by 0.09 V for $[Ir(C\text{^}N)_2(pytpy)]^+$. The increase in $E^{ox}_{1/2}$ on going from $[Ir(dmppz)_2(pytpy)]^+$ to $[Ir(dmppz)_2(Mepytpy)]^{2+}$ is consistent with the increase in overall positive charge on the complex. At least one ligand-based reduction is observed for each complex. These processes are expected to be based on the tpy domain since the LUMO of the complex is localized on the N^N ligand.

Solution photophysical properties

The electronic absorption spectra of the $[Ir(ppy)_2(N\text{^}N)]^+$, $[Ir(dmppz)_2(N\text{^}N)]^+$ and $[Ir(dmppz)_2(Mepytpy)]^{2+}$ complexes are shown in Fig. 7. The spectra are dominated by intense bands in the UV region assigned to C^N and N^N ligand-based $\pi^*\leftarrow\pi$ and $\pi^*\leftarrow$n transitions. The presence of the 4′-aryl or 4′-pyridyl unit extends the π-conjugation, leading to enhanced intensities of absorptions in $[Ir(ppy)_2(N\text{^}N)]^+$ (N^N = **1–4**, pytpy) and $[Ir(dmppz)_2(N\text{^}N)]^+$ (N^N = pytpy, $[Mepytpy]^+$) compared to those in $[Ir(ppy)_2(tpy)]^+$ and $[Ir(dmppz)_2(tpy)]^+$.

The photoluminescence (PL) spectra of CH_2Cl_2 solutions of $[Ir(ppy)_2(N\text{^}N)][PF_6]$ and $[Ir(dmppz)_2(N\text{^}N)][PF_6]$ are shown in Fig. 8, and PL data are given in Table 5. The iridium(III) complexes containing neutral, tpy-based ligands are orange or red

Table 4 Cyclic voltammetric data with respect to Fc/Fc^+; CH_2Cl_2 solutions with $[^nBu_4N][PF_6]$ supporting electrolyte, and scan rate of 0.1 V s^{-1} (ir = irreversible; qr = quasi-reversible)

Compound	$E^{ox}_{1/2}$/V	$E^{red}_{1/2}$/V	$\Delta E_{1/2}$/V
$[Ir(ppy)_2(tpy)][PF_6]$	$+0.90^{ir}$	-1.82^{qr}	2.72
$[Ir(ppy)_2(\mathbf{1})][PF_6]$	$+0.75^{ir}$	-1.86^{qr}, -2.15^{ir}	2.61
$[Ir(ppy)_2(\mathbf{2})][PF_6]$	$+0.77^{qr}$	-1.85^{qr}	2.62
$[Ir(ppy)_2(\mathbf{3})][PF_6]$	$+0.84^{ir}$	-1.82^{qr}	2.66
$[Ir(ppy)_2(\mathbf{4})][PF_6]$	$+0.74^{ir}$	-1.74^{ir}, -2.05^{qr}	2.48
$[Ir(ppy)_2(pytpy)][PF_6]$	$+0.88^{ir}$	-1.71^{qr}	2.59
$[Ir(dmppz)_2(tpy)][PF_6]$	$+0.82^{ir}$	-1.87^{qr}	2.69
$[Ir(dmppz)_2(pytpy)][PF_6]$	$+0.79^{qr}$	-1.71^{qr}	2.50
$[Ir(dmppz)_2(Mepytpy)][PF_6]_2$	$+0.88^{qr}$	-1.30^{qr}, -2.07^{ir}	2.18

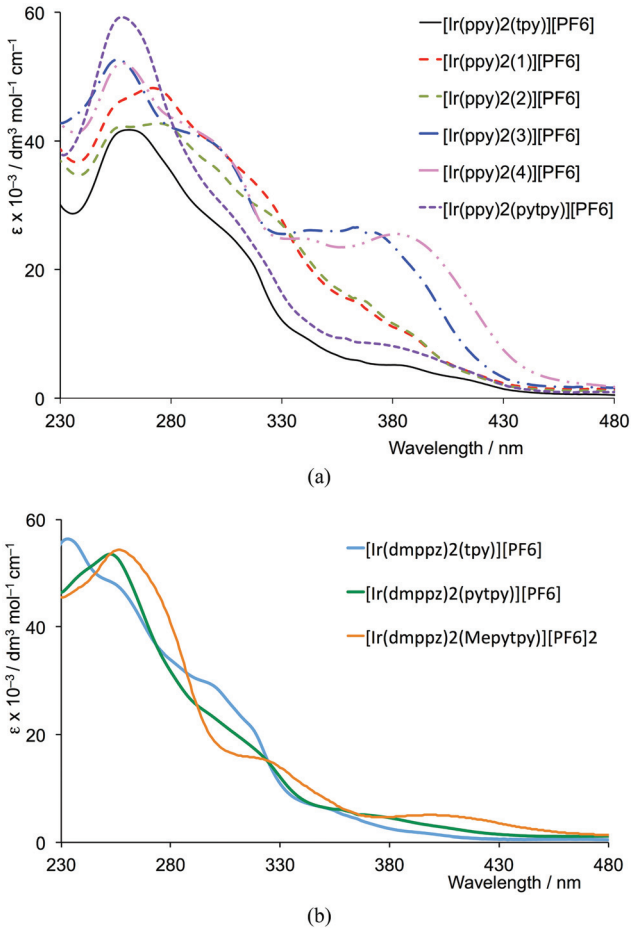

Fig. 7 Absorption spectra of CH_2Cl_2 solutions of (a) $[Ir(ppy)_2(N\text{^}N)][PF_6]$ and (b) $[Ir(dmppz)_2(N\text{^}N)][PF_6]_n$ (n = 1 for N^N = tpy and pytpy; n = 2 for N^N = $[Mepytpy]^+$).

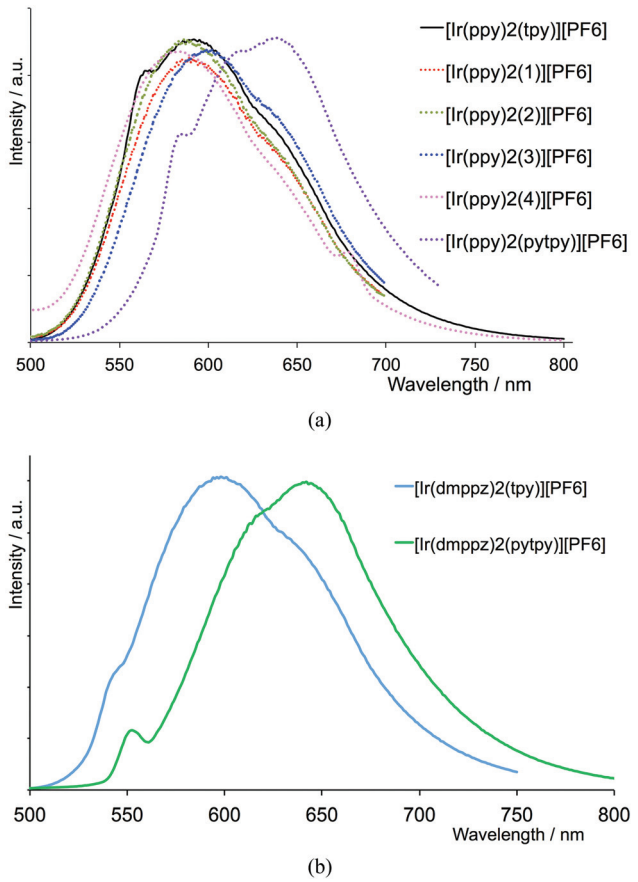

Fig. 8 Solution photoluminescence spectra of CH_2Cl_2 solutions of (a) $[Ir(ppy)_2(N^N)][PF_6]$ and (b) $[Ir(dmppz)_2(N^N)][PF_6]$.

emitters, and the emission bands are broad and unstructured. The parent complex $[Ir(ppy)_2(tpy)]^+$ emits at 590 nm, but exhibits a very low quantum yield and a lifetime of 68 ns (Table 5). The emission maximum is little shifted on introducing 4′-C_6H_4X (X = OH, OMe, SMe, NH_2) substituents into the tpy domain or by replacing $[ppy]^-$ by $[dmppz]^-$. However, the quantum yields and lifetimes are enhanced (Table 5), the two best being 9.9% and 125 ns for $[Ir(ppy)_2(\mathbf{4})][PF_6]$, and 7.5% and 136 ns for $[Ir(dmppz)_2(tpy)][PF_6]$. A significant red shift in the emission is observed on going from $[Ir(ppy)_2(tpy)][PF_6]$ to $[Ir(ppy)_2(pytpy)][PF_6]$ ($\Delta\lambda$ = 50 nm), or from $[Ir(dmppz)_2(tpy)][PF_6]$ to $[Ir(dmppz)_2(pytpy)][PF_6]$ ($\Delta\lambda$ = 43 nm). This is consistent with the observed decrease in the electrochemical bandgaps for these pairs of compounds (Table 4). The effect of N-methylation on going from $[Ir(dmppz)_2(pytpy)][PF_6]$ to $[Ir(dmppz)_2(Mepytpy)][PF_6]_2$ is to virtually quench the emission.

Electroluminescence and device performances

LECs were prepared of all complexes in the thin film configuration described in the Experimental section. However, for $[Ir(dmppz)_2(pytpy)][PF_6]$, film formation was not sufficiently good to permit a detailed investigation. Even though the performance of some of the devices was poor, especially when

Table 5 Solution (degassed CH_2Cl_2) photoluminescence data for the iridium(III) complexes

Compound	λ_{exc}/nm	λ_{max}^{em}/nm	$\tau_{1/2}$[a]/ns	QY/%
$[Ir(ppy)_2(tpy)][PF_6]$	260	590	68	1.7
$[Ir(ppy)_2(\mathbf{1})][PF_6]$	360	590	93	5.8
$[Ir(ppy)_2(\mathbf{2})][PF_6]$	320	589	98	6.1
$[Ir(ppy)_2(\mathbf{3})][PF_6]$	325	595	87	6.8
$[Ir(ppy)_2(\mathbf{4})][PF_6]$	255	580	125	9.9
$[Ir(ppy)_2(pytpy)][PF_6]$	250	640	54	2.9
$[Ir(dmppz)_2(tpy)][PF_6]$	250	599	136	7.5
$[Ir(dmppz)_2(pytpy)][PF_6]$	256	642	119	6.2

[a] Solutions were degassed with argon for 15 min; lifetime measurements were made under argon.

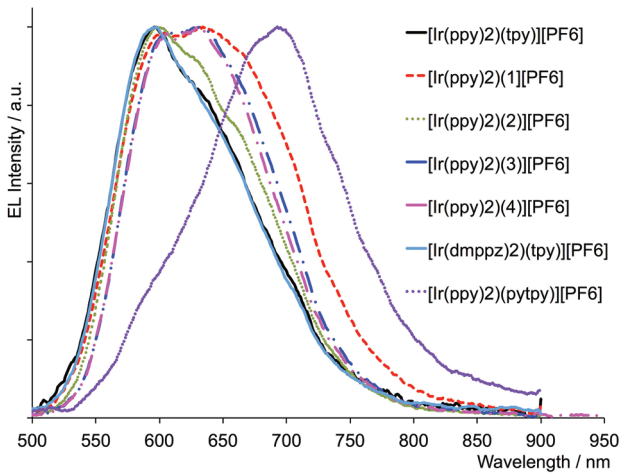

Fig. 9 Electroluminescence spectra for ITO/PEDOT : PSS/[Ir-iTMC]/IL (4 : 1)/Al LECs biased by a pulsed current of 100 A m^{-2} (1000 Hz, 50% duty cycle, block wave), except for devices employing complexes $[Ir(ppy)_2(tpy)][PF_6]$, $[Ir(ppy)_2(\mathbf{4})][PF_6]$, $[Ir(dmppz)_2(tpy)][PF_6]$ (measured at 150 A m^{-2}) and $[Ir(ppy)_2(pytpy)][PF_6]$ (measured at 300 A m^{-2}).

compared with that of the archetypal iTMC $[Ir(ppy)_2(6\text{-Phbpy})]^+$ (see Fig. S11†), we were able to obtain the electroluminescent spectra for all the complexes and these are shown in Fig. 9. Electroluminescence (EL) maxima are compared with PL data in Table 6. The emission spectra of all LECs are red-shifted with respect to the PL spectra of the corresponding Ir-iTMC in thin film configuration. It is noteworthy that the EL maximum is red-shifted with respect to the archetypal iTMC $[Ir(ppy)_2(6\text{-Phbpy})][PF_6]$[3] leading to interesting red-emitting devices. Such a red shift is frequently observed in LECs and may be related to the location of the emission zone in the devices. However, the shift observed in the device based on $[Ir(ppy)_2(pytpy)][PF_6]$ is exceptionally large which indicates a different emitting state involved.[40] Note that that particular device showed weak electroluminescence even at higher applied current densities. Due to this, no further investigation as to the origin of the large shift in the emission spectrum was carried out.

The most efficient devices were those employing the complexes $[Ir(ppy)_2(\mathbf{1})][PF_6]$, $[Ir(ppy)_2(\mathbf{2})][PF_6]$ and $[Ir(ppy)_2(\mathbf{3})]$-

Table 6 Photoluminescence in thin film (iTMC : IL 4 : 1) and electroluminiscence data for LECs: ITO/PEDOT : PSS/iTMC : IL 4 : 1/Al biased by a pulsed current of 100 A m^{-2} (1000 Hz, 50% duty cycle, block wave). PL spectra are shown in Fig. S12

Compound	PL λ_{max}/nm	PLQY/%	Turn-on time (t_{on})/min	Luminance$_{max}$/cd m^{-2}	EL λ_{max}/nm	EQE/%
$[Ir(ppy)_2(tpy)][PF_6]$	590	11.8	<1	11	598[b]	<0.1
$[Ir(ppy)_2(\mathbf{1})][PF_6]$	593	11.3	<1	60	625	0.4
$[Ir(ppy)_2(\mathbf{2})][PF_6]$	591	23.5	3.6	54	602	0.3
$[Ir(ppy)_2(\mathbf{3})][PF_6]$	604	15.8	6	29	620	0.2
$[Ir(ppy)_2(\mathbf{4})][PF_6]$	600	4.6	<1	1	632[b]	<0.1
$[Ir(ppy)_2(pytpy)][PF_6]$	641	4.8	—	—	695[a]	—
$[Ir(dmppz)_2(tpy)][PF_6]$	597	8.7	30	11	600[b]	<0.1
$[Ir(dmppz)_2(pytpy)][PF_6]$	637	6.6	—	—	—	—

[a] Measured under an average current density of 300 A m^{-2}. [b] Measured under an average current of 150 A m^{-2}.

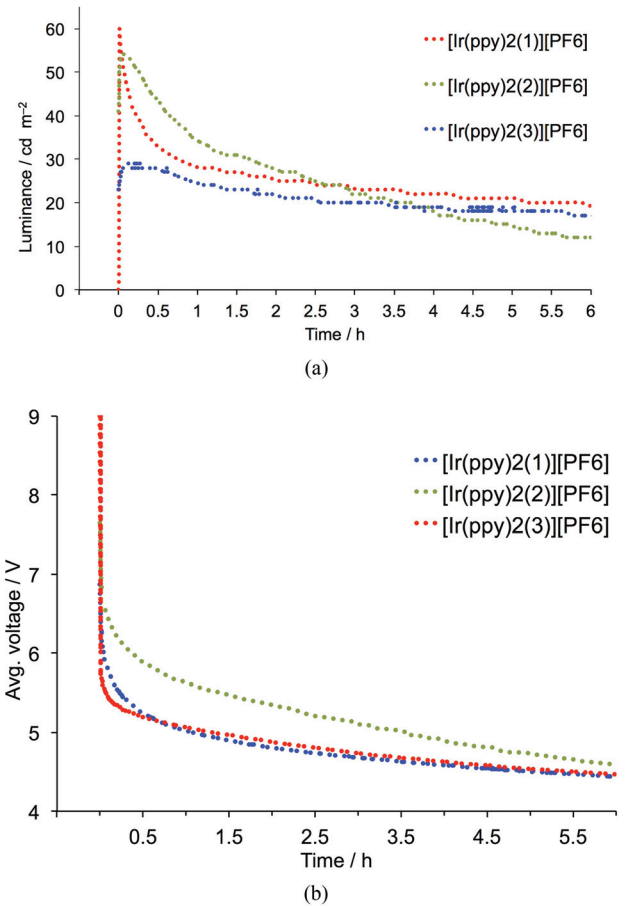

Fig. 10 (a) Luminance and (b) average voltage *versus* time for ITO/PEDOT : PSS/[Ir-iTMC]/IL(4 : 1)/Al LECs biased by a pulsed current of 100 A m^{-2} (1000 Hz, 50% duty cycle, block wave).

$[PF_6]$. The transient luminance and driving voltage of these devices are depicted in Fig. 10. For all three devices the turn-on is very rapid, in part due to the pulsed current driving applied and in part due to the presence of the ionic liquids in the emitting layer.[41,42] The voltage required to sustain the applied current density of 100 A m^{-2} decreases rapidly over the first few minutes. This demonstrates the reduction of the injection barrier for electrons and/or holes as the ions accumulate at the device interface. With increasing time, the voltage continues to decrease but at a slower speed. This coincides with a gradual decrease in the luminance with a similar slope as that observed for the voltage decrease. Hence, this is a signature of progression of the doped regions towards the interior of the emissive film.[43] This broadening of the doped regions leads to decreasing intrinsic film thickness. Hence, it requires a lower voltage to maintain the applied current density but also more excitons are quenched by the increased number of doping sites. The efficiency of the LECs is not very high, in spite of the reasonable PLQY observed for some of the complexes, measured in device configuration of iTMC : IL 4 : 1 molar ratio. This low efficiency indicates that the device performance is not optimal, and this is probably related to an imbalance in charge carriers.

Conclusions

We have prepared and characterized a series of $[Ir(C\hat{}N)_2(N\hat{}N)][PF_6]$ complexes in which the cyclometallating ligand, C^N, is either ppy^- or $dmppz^-$, and the N^N chelate is a tpy or a derivative thereof. Solution NMR spectroscopic data reveal that (i) the pendant pyridine ring of the coordinated tpy undergoes hindered rotation and (ii) in the $[Ir(ppy)_2(N\hat{}N)]^+$ complexes, the non-coordinated N-donor of the pendant pyridine ring forms a non-classical hydrogen bond with a CH unit of one pyridine ring of an adjacent ppy^- ligand. The single crystal structures of eight complexes have been elucidated, and confirm that a general feature is intra-cation face-to-face π-stacking of the non-coordinated pyridine ring of the tpy domain with the cyclometallated ring. In CH_2Cl_2, the complexes are orange or red emitters, with λ_{max}^{em} in the range 580 to 642 nm. Quantum yields are <10%, and the emission lifetimes range from 54 to 136 ns. LECs have been fabricated using the new Ir-iTMCs, and the emission spectra of the LECs are red-shifted with respect to the photoluminescence spectra of the corresponding complex in thin film configuration. For the device incorporating $[Ir(ppy)_2(pytpy)][PF_6]$, the PL to EL red-shift is especially large, indicating that a different emitting state is involved. The most efficient devices investigated were $[Ir(ppy)_2(\mathbf{1})][PF_6]$, $[Ir(ppy)_2(\mathbf{2})][PF_6]$ and $[Ir(ppy)_2(\mathbf{3})][PF_6]$; the

devices exhibited rapid turn-on times, but displayed relatively low efficiencies.

Acknowledgements

We thank the European Research Council (Advanced Grant 267816 LiLo), the Swiss National Science Foundation, and the University of Basel for financial support, the Spanish Ministry of Economy and Competitiveness (MINECO) (MAT2011-24594, CTQ2009-08790 and Consolider-Ingenio CSD2007-00010), the Generalitat Valenciana (PROMETEO/2012/053) and the European Union (CELLO, STRP 248043; https://www.cello-project.eu/) for financial support. C.R. acknowledges the Spanish Ministry of Education, Culture, and Sport for an FPU grant. A.P. also acknowledges MINECO for an FPI grant. Nik Hostettler and Jonas Schönle are thanked for recording 500 MHz NMR spectra.

Notes and references

1 E. Baranoff, J.-H. Yum, M. Graetzel and Md. K. Nazeeruddin, *J. Organomet. Chem.*, 2009, **694**, 2661.
2 R. D. Costa, E. Ortí, H. J. Bolink, F. Monti, G. Accorsi and N. Armaroli, *Angew. Chem., Int. Ed.*, 2012, **51**, 8178.
3 H. J. Bolink, E. Coronado, R. D. Costa, E. Ortí, M. Sessolo, S. Graber, K. Doyle, M. Neuburger, C. E. Housecroft and E. C. Constable, *Adv. Mater.*, 2008, **20**, 3910.
4 S. Graber, K. Doyle, M. Neuburger, C. E. Housecroft, E. C. Constable, R. D. Costa, E. Ortí, D. Repetto and H. J. Bolink, *J. Am. Chem. Soc.*, 2008, **130**, 14944.
5 R. D. Costa, E. Ortí, H. J. Bolink, S. Graber, C. E. Housecroft, M. Neuburger, S. Schaffner and E. C. Constable, *Chem. Commun.*, 2009, 2029.
6 R. D. Costa, E. Ortí, H. J. Bolink, S. Graber, C. E. Housecroft and E. C. Constable, *Adv. Funct. Mater.*, 2010, **20**, 1511.
7 F. Neve, A. Crispini, S. Campagna and S. Serroni, *Inorg. Chem.*, 1999, **38**, 2250.
8 F. Neve and A. Crispini, *Eur. J. Inorg. Chem.*, 2000, 1039.
9 M. Lepeltier, T. K.-M. Lee, K. K.-W. Lo, L. Toupet, H. Le Bozec and V. Guerchais, *Eur. J. Inorg. Chem.*, 2005, 110.
10 J. O. Huh, M. H. Lee, H. Jang, K. Y. Hwang, J. S. Lee, S. H. Kim and Y. Do, *Inorg. Chem.*, 2008, **47**, 6566.
11 R. D. Costa, E. Ortí, H. J. Bolink, S. Graber, C. E. Housecroft and E. C. Constable, *J. Am. Chem. Soc.*, 2010, **132**, 5978.
12 R. D. Costa, E. Ortí, H. J. Bolink, S. Graber, C. E. Housecroft and E. C. Constable, *Chem. Commun.*, 2011, **47**, 3207.
13 A. M. Bünzli, H. J. Bolink, E. C. Constable, C. E. Housecroft, M. Neuburger, A. Pertegás and J. A. Zampese, *Eur. J. Inorg. Chem.*, 2012, 3780.
14 E. Baranoff, H. J. Bolink, E. C. Constable, M. Delgado, D. Häussinger, C. E. Housecroft, M. K. Nazeeruddin, M. Neuburger, E. Ortí, G. E. Schneider, D. Tordera, R. M. Walliser and J. A. Zampese, *Dalton Trans.*, 2013, **42**, 1073.
15 D. Tordera, A. M. Bünzli, A. Pertegás, J. M. Junquera-Hernández, E. C. Constable, J. A. Zampese, C. E. Housecroft, E. Ortí and H. J. Bolink, *Chem.–Eur. J.*, 2013, **19**, 8597.
16 R. D. Costa, E. Ortí, H. J. Bolink, S. Graber, S. Schaffner, M. Neuburger, C. E. Housecroft and E. C. Constable, *Adv. Funct. Mater.*, 2009, **19**, 3456.
17 F. Neve, M. La Deda, F. Puntoriero and S. Campagna, *Inorg. Chim. Acta*, 2006, **359**, 1666.
18 F. H. Allen, *Acta Crystallogr., Sect. B: Struct. Sci.*, 2002, **58**, 380.
19 I. J. Bruno, J. C. Cole, P. R. Edgington, M. Kessler, C. F. Macrae, P. McCabe, J. Pearson and R. Taylor, *Acta Crystallogr., Sect. B: Struct. Sci.*, 2002, **58**, 389.
20 L. He, J. Qiao, L. Duan, G. Dong, D. Zhang, L. Wang and Y. Qiu, *Adv. Funct. Mater.*, 2009, **19**, 2950.
21 H.-C. Su, H.-F. Chen, F.-C. Fang, C.-C. Liu, C.-C. Wu, K.-T. Wong, Y.-H. Liu and S.-M. Peng, *J. Am. Chem. Soc*, 2008, 130, 3413.
22 J. L. Rodríguez-Redondo, R. D. Costa, E. Ortí, A. Sastre-Santos, H. J. Bolink and F. Fernández-Lázaro, *Dalton Trans.*, 2009, 9787.
23 J. Zhang, L. Zhou, H. A. Al-Attar, K. Shao, L. Wang, D. Zhu, Z. Su, M. R. Bryce and A. P. Monkman, *Adv. Funct. Mater.*, 2013, **23**, 4667.
24 K. T. Potts, P. Ralli, G. Theodoridis and P. Winslow, *Org. Synth.*, 1986, **64**, 189.
25 J. Wang and G. S. Hanan, *Synlett*, 2005, 1251.
26 E. C. Constable, C. E. Housecroft, M. Neuburger, D. Phillips, P. R. Raithby, E. Schofield, E. Sparr, D. A. Tocher, M. Zehnder and Y. Zimmermann, *J. Chem. Soc., Dalton Trans.*, 2000, 2219.
27 E. C. Constable, C. E. Housecroft, E. Medleycott, M. Neuburger, F. Reinders, S. Reymann and S. Schaffner, *Inorg. Chem. Commun.*, 2008, **11**, 518.
28 G. D. Storrier, S. B. Colbran and D. C. Craig, *J. Chem. Soc., Dalton Trans.*, 1997, 3011.
29 S. Sprouse, K. A. King, P. J. Spellane and R. J. Watts, *J. Am. Chem. Soc.*, 1984, **106**, 6647.
30 APEX2, version 2 User Manual, M86-E01078, Bruker Analytical X-ray Systems, Inc., Madison, WI, 2006.
31 Stoe & Cie, *IPDS software v 1.26*, Stoe & Cie, Darmstadt, Germany, 1996.
32 G. M. Sheldrick, *Acta Crystallogr., Sect. A: Fundam. Crystallogr.*, 2008, **64**, 112.
33 I. J. Bruno, J. C. Cole, P. R. Edgington, M. K. Kessler, C. F. Macrae, P. McCabe, J. Pearson and R. Taylor, *Acta Crystallogr., Sect. B: Struct. Sci.*, 2002, **58**, 389.
34 C. F. Macrae, I. J. Bruno, J. A. Chisholm, P. R. Edgington, P. McCabe, E. Pidcock, L. Rodriguez-Monge, R. Taylor, J. van de Streek and P. A. Wood, *J. Appl. Crystallogr.*, 2008, **41**, 466.
35 See for example ref. 7 and references cited therein.
36 C. Janiak, *J. Chem. Soc., Dalton Trans.*, 2000, 3885.

37 See for example: E. C. Constable and A. W. M. Cargill Thompson, *J. Chem. Soc., Dalton Trans.*, 1994, 1409; S. Silvi, E. C. Constable, C. E. Housecroft, J. E. Beves, E. L. Dunphy, M. Tomasulo, F. M. Raymo and A. Credi, *Chem.–Eur. J.*, 2009, **15**, 178; M. G. Lobello, S. Fantacci, A. Credi and F. De Angelis, *Eur. J. Inorg. Chem.*, 2011, 1605.
38 K. J. Arm, W. Leslie and J. A. G. Williams, *Inorg. Chim. Acta*, 2006, **359**, 1222.
39 R. D. Costa, E. Ortí, D. Tordera, A. Pertegás, H. J. Bolink, S. Graber, C. E. Housecroft, L. Sachno, M. Neuburger and E. C. Constable, *Adv. Energy Mater.*, 2011, **1**, 282.
40 H. J. Bolink, L. Cappelli, S. Cheylan, E. Coronado, R. D. Costa, N. Lardies, M. K. Nazeeruddin and E. Orti, *J. Mater. Chem.*, 2007, **17**, 5032.
41 S. T. Parker, J. D. Slinker, M. S. Lowry, M. P. Cox, S. Bernhard and G. G. Malliaras, *Chem. Mater.*, 2005, **17**, 3187.
42 D. Tordera, S. Meier, M. Lenes, R. D. Costa, E. Orti, W. Sarfert and H. J. Bolink, *Adv. Mater.*, 2012, **24**, 897.
43 M. Lenes, G. García-Belmonte, D. Tordera, A. Pertegás, J. Bisquert and H. J. Bolink, *Adv. Funct. Mater.*, 2011, **21**, 1581.